Title page

Title

Release of the pre-assembled naRNA-LL37 composite DAMP re-defines neutrophil extracellular traps (NETs) as intentional DAMP webs

Running title

naRNA – canonical NET component and composite DAMP

Authors

Francesca Bork[1], Carsten L. Greve[1], Christine Youn[2], Sirui Chen[1], Yu Wang[2], Masoud Nasri[3], Jule Focken[4], Jasmin Scheurer[4], Pujan Engels[1], Marissa Dubbelaar[1,5], Katharina Hipp[6], Birgit Schittek[4,7,8], Stefanie Bugl[1], Markus W. Löffler[1,7,9], Julia Skokowa[3,7], Nathan K. Archer[2] (ORCID: 0000-0002-8212-8985), Alexander N.R. Weber[1,7,8]* (ORCID: 0000-0002-8627-7056)

Author information

[1]Interfaculty Institute for Cell Biology, Department of Immunology, University of Tübingen, Auf der Morgenstelle 15, 72076 Tübingen, Germany

[2]Department of Dermatology, Johns Hopkins University School of Medicine, Baltimore, MD 21231, USA

[3]Division of Translational Oncology, Department of Oncology, Hematology, Clinical Immunology and Rheumatology, University Hospital Tübingen, Otfried-Müller Str. 10, 72076 Tübingen, Germany

[4]Division of Dermato-oncology, Department of Dermatology, University Hospital Tübingen, Liebermeisterstr. 25, 72076 Tübingen, Germany

[5]Quantitative Biology Center (QBiC), University of Tübingen, Auf der Morgenstelle 10, 72076 Tübingen, Germany

[6]Electron Microscopy Facility, Max Planck Institute for Biology Tübingen, Max-Planck-Ring 5, 72076 Tübingen, Germany

28 [7]iFIT – Cluster of Excellence (EXC 2180) "Image-Guided and Functionally Instructed Tumor Therapies",
29 University of Tübingen, Germany

30 [8]CMFI – Cluster of Excellence (EXC 2124) "Controlling microbes to fight infection", University of
31 Tübingen, Germany.

32 [9]Department of General, Visceral and Transplant Surgery, University Hospital Tübingen, Hoppe-
33 Seyler-Str. 3, 72076 Tübingen, Germany and Department of Clinical Pharmacology, University
34 Hospital Tübingen, Auf der Morgenstelle 8, 72076 Tübingen, Germany

35

36 **Corresponding Author**

37 Alexander N. R. Weber, Interfaculty Institute for Cell Biology, Department of Immunology, University
38 of Tübingen, Auf der Morgenstelle 15, 72076 Tübingen, Germany. Tel.: +49 7071 29 87623. Fax: +49
39 7071 29 4579. Email: alexander.weber@uni-tuebingen.de; ORCID: 0000-0002-8627-7056, Twitter
40 @aweberlab

Abstract

Neutrophil extracellular traps (NETs) are a key antimicrobial feature of cellular innate immunity mediated by polymorphonuclear neutrophils (PMNs), the primary human leukocyte population. NETs trap and kill microbes but have also been linked to inflammation, e.g. atherosclerosis, arthritis or psoriasis by unknown mechanisms. We here characterize naRNA (NET-associated RNA), as a new canonical, abundant, and unexplored inflammatory NET component. naRNA, upon release by NET formation, drove further NET formation in naïve PMN, and induced macrophage and keratinocyte activation via TLR8 in humans and Tlr13 in mice, in vitro and in vivo. Importantly, in vivo naRNA strongly drove skin inflammation, whereas genetic ablation of RNA sensing drastically ameliorated psoriatic skin inflammation. Rather than accidentally assembling with LL37 on the NET, naRNA was intracellularly pre-associated in resting neutrophils as a 'composite DAMP', thus highlighting NET formation as a DAMP release process. This re-defines sterile NETs as an intentionally inflammatory agent, signaling and amplifying neutrophil activation. Moreover, in the many conditions previously linked to NETs and extracellular RNA, TLR-mediated naRNA sensing emerges as both potential cause and new intervention target.

Graphical abstract

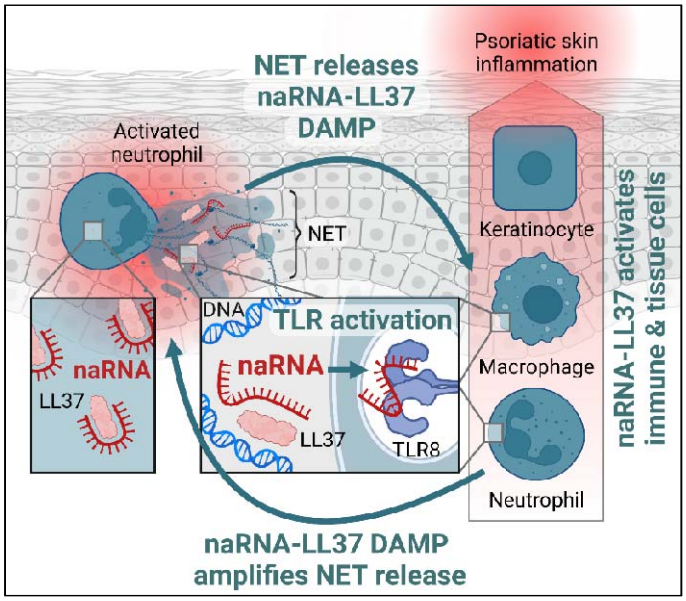

Created with biorender.com

59 **Introduction**

60 The formation of Neutrophil Extracellular Traps (NETs), since its discovery in 2004 (*1*), has emerged
61 as a fascinating phenomenon of host defense. Hereby neutrophils, the primary leukocyte population,
62 extrude their genomic DNA to form web-like structures that, similar to barbed wire roadblocks, trap
63 and kill microbial invaders such as bacteria or fungi (*2*). DNA is thus a defining structural and
64 functional feature of NETs. Additionally, DNA-associated proteins, histones and HMGB-1,
65 antimicrobial peptides like LL37 and enzymes such as myeloperoxidase (MPO) are released during
66 the formation of NETs and contribute to their antimicrobial function (*2*). With their primary role
67 firmly established to be antimicrobial, the reported role of NETs in sterile inflammatory conditions
68 such as atherosclerosis (*3*), rheumatoid arthritis (RA) (*4*) and COVID-19 (*5*) has remained somewhat
69 enigmatic, but generally an accidental phenomenon. Specifically, the observed inflammation-
70 promoting effects of sterile NETs have not been mechanistically linked to a specific component of
71 NETs, despite the fact that >1,000 publications on NETs have sought to detail the multi-faceted
72 phenomenon and the processes that lead to its execution (*6*). However, with the main focus devoted
73 to DNA and protein components, another primary cellular biomolecule, RNA, has so far received very
74 little attention in vertebrates. Interestingly, a study in insects showed that hemocytes (macrophage-
75 like immune cells) can release both DNA and RNA in NET-like structures during microbe-triggered
76 clotting reactions, and in response to extracellular RNA or DNA (*7*). Our lab recently provided
77 evidence of a responsiveness of human polymorphonuclear neutrophils (PMNs) to RNA, but not DNA,
78 in combination with the antimicrobial peptide LL37 (*8*). In addition, earlier work described a role for
79 DNA- and RNA-LL37 complexes in the activation of plasmacytoid dendritic cells (*9, 10*). This has given
80 rise to the notion that under certain conditions tolerance to self-DNA and RNA 'accidentally', e.g. in
81 psoriasis patients, can be broken by LL37 (*11*), involving the nucleic acid-sensing TLR7, TLR8 (ssRNA)
82 and TLR9 (DNA) in humans, and Tlr7, Tlr13 and Tlr9 in mice (*12, 13*). In general, many roles have been
83 ascribed to so-called extracellular RNA (exRNA), for example, macrophage polarization, recruitment
84 of leukocytes to the site of inflammation, leukocyte rolling at the vascular endothelium, as well as
85 integrin-mediated firm adhesion of immune cells and promotion of thrombosis (*14*). Additionally,
86 exRNA is considered as a reliable biomarker for various diseases such as cancer or cardiovascular
87 pathologies (*15, 16*). However, RNA being considered a short-lived biomolecule, physiological sources
88 of exRNA have been somewhat unclear. Under sterile conditions, vascular injury, tissue damage, or
89 ischemia have been suggested to trigger release of exRNA along with other cellular material (*14*) but
90 it remains unclear whether these relatively slow processes could amount to physiologically
91 detectable exRNA amounts in the serum of patients, or whether a rapid, as-yet unidentified process
92 of RNA extrusion would have to be postulated.

93 We show here that RNA contained in NETs, so-called NET-associated RNA or naRNA, drives such a
94 self-amplifying inflammatory loop not only engaging PMNs but also macrophages and keratinocytes.
95 naRNA responsiveness was dependent on *TLR8* and *Tlr13* in human and murine myeloid immune
96 cells, respectively. Notably, in mice naRNA caused considerable skin inflammation in a Tlr13-
97 dependent manner and in a well-established model of psoriatic skin inflammation, genetic ablation
98 of RNA sensing strongly ameliorated skin inflammation. Importantly, the observed pre-association of
99 naRNA with LL37 in resting neutrophils from healthy donors indicates that NETs are strictly intended
100 for extrusion of this novel 'composite' DAMP. Not only does this show that the presumed 'breaking
101 of tolerance' by LL37 is non-accidental. As the majority of pathological conditions in which NETs have
102 been described in are sterile, our data re-define the primary purpose of NET formation to be DAMP
103 release, with naRNA-LL37 acting as a molecular beacon to report on PMN activation and alert tissue
104 and other immune cells.

105 ## Results

106 **naRNA is a common component of NETs**

107 To first investigate whether naRNA was a common component of NETs, we compared NETs from
108 human PMNs formed in response to the well-defined molecular agonists PMA, different complexes
109 of LL37 with purified RNA (synthetic, as well as total fungal and bacterial RNA from *S. aureus* and *C.*
110 *albicans*, respectively), nigericin and the live pathogen *C. albicans*. Confocal microscopy analysis
111 using the well-characterized rRNA-specific antibody, Y10b (*17*), revealed the presence of RNA in all
112 corresponding NETs, independent of stimulus and whether NET formation was 'suicidal' or not (*6*)
113 (Fig. 1A, quantified in B; control in Fig. S1A): the RNA signal was readily detectable along the web-like
114 DNA threads in human NETs. Similar results were obtained in NETs released by murine bone marrow-
115 derived PMNs (BM-PMNs, Fig. 1C; control Fig. S1B). To avoid the use of staining reagents, we also
116 metabolically labeled primary human hematopoietic stem cells (HSCs) with 5-ethynyluridine (5-EU), a
117 nucleotide that can be incorporated in cellular RNA but not DNA, and that is amenable to labeling by
118 click chemistry (*18*). These HSCs were then differentiated to neutrophils (*19*) and the differentiation
119 validated by microscopy and flow cytometric analysis (Fig. S1C, D). NETs released from HSC-derived
120 PMNs could indeed be labeled with click reagents conferring a fluorescent label only when grown in
121 5-EU-containing medium (Fig. 1D). Moreover, the overlap between click-label and rRNA confirmed
122 the specificity of the staining with anti-rRNA antibodies and indicated that naRNA contained rRNA
123 but also other types of cellular RNAs. This experiment also unequivocally confirmed that upon PMN
124 stimulation, cellular RNA is turned into a component of the NET, wherein it decorates the fine, web-
125 like DNA structures. The localization of naRNA on DNA strands was further confirmed by high-
126 resolution fluorescence microscopy and 3D analysis (AiryScan, Fig. 1E and Supplemental Movie S1) as

127 well as scanning electron microscopy (SEM, Fig. 1F; controls Fig. S1E). Extraction of naRNA from PMA-
128 induced NETs (Fig. 1G) and subsequent RNA-sequencing analysis confirmed that purified naRNA
129 contained multiple RNA types, with noticeably more non-ribosomal RNA than the corresponding
130 total cellular RNA of PMNs (Fig. 1H). Collectively, these results indicate that naRNA is a canonical
131 component of NETs released upon multiple stimuli from both human and murine neutrophils.

132 **naRNA is a potent 'composite' DAMP propagating NET formation in primary PMNs**

133 A primary function of NETs is host defense by trapping and killing bacteria. Therefore, we first
134 explored if naRNA participated in this process (*1*). However, the antibacterial effect of NETs on live
135 *Staphylococcus aureus* (evidenced by lower CFUs compared to resting PMNs) was similar to that of
136 RNase-treated NETs, whereas DNase digestion reduced the drop in CFU discernibly but non-
137 significantly (Fig. S2A). Consequently, we turned our attention to a possible role of naRNA as a
138 DAMP, since primary PMNs can respond to synthetic RNA-LL37 complexes with NET formation, and
139 our earlier analysis indicated that NETs also contain LL37 (*8*). To prepare a naRNA-containing
140 stimulant, PMA-induced NETs were prepared as described in Methods and the original stimulus,
141 PMA, removed by extensive washing before harvesting (Fig. 2A). Interestingly, these 'PMA NETs',
142 when applied to naïve PMNs from another donor, potently induced new NETs (Fig. 2B, quantified in
143 C, controls in Fig. S2B). Treatment with an RNase inhibitor enhanced the stimulatory effect of PMA
144 NETs rendering a 1:500 dilution of PMA-NETs more effective than a 1:50 dilution of non-treated
145 PMA-NETs (Fig. 2B, C, controls Fig. S2B). Interestingly, similar NET preparations from mock-treated
146 PMNs (here referred to as 'mock NETs') did not stimulate NET formation under the same
147 experimental conditions. To rule out the possibility that residual PMA in PMA NETs could be
148 responsible for the observed stimulatory effects, RNase treatment was also performed which
149 strongly reduced NET formation (Fig. 2D, quantified in E; controls Fig. S2C). The destruction of naRNA
150 in NETs was further confirmed by rapid loss of the RNA signal (using the RNA-selective dye, SYTO
151 RNAselect (*8*) in time-lapse digestion analysis (Supplemental Movie S2). Bearing in mind that PMNs
152 do not respond to DNA or DNA-LL37 complexes (*8*), the opposing effects of RNase inhibitor and
153 RNase treatments thus clearly indicated naRNA (and not DNA) to be the relevant immunostimulatory
154 component for NETs to drive the activation of naïve PMNs. In line with our previous work showing
155 that synthetic RNA or LL37 alone cannot trigger PMN activation (*8*), purified 'naked' (i.e. (stripped of
156 DNA or proteins) naRNA isolated from PMA NETs (*cf.* Fig. 1G) was unable to activate NET formation;
157 however, re-complexing with exogenous LL37 was sufficient to restore NET formation (Fig. 2F,
158 controls in Fig. S2D). naRNA (*cf.* Fig. 2F) and LL37 (*8*) on their own are thus not DAMPs but, in the
159 context of NETs, act in concert as a novel type of 'composite' DAMP.

160 **naRNA DAMP activity is dependent on RNA sensors TLR8/Tlr13**

161 To validate naRNA as an immunostimulatory RNA component from the receptor side, we turned to
162 HEK293T cells which do not respond to RNA, unless transfected with plasmids encoding the human
163 ssRNA sensors TLR7 or TLR8 (*20*). NF-κB reporter assays revealed that TLR7 or TLR8- (both ssRNA
164 sensors) but not TLR9 (human DNA sensor)-transfected HEK293T cells stimulated with PMA NETs or
165 mock NETs showed robust NF-κB activity only for PMA NETs (Fig. 3A). R848 (TLR7 and TLR8 agonist)
166 and TL8 or ssRNA+DOTAP (both TLR8 agonists) served as controls. Of note, compared to its cognate
167 agonist, CpG, the DNA sensor TLR9 was only poorly activated by PMA NETs, indicating that naRNA is a
168 superior immune stimulant compared to NET DNA in this system. Indeed, the observed NET response
169 of primary PMNs (Fig. 3B, quantified in C, and Fig. S3A) could be completely blocked by the TLR8-
170 specific inhibitor, CU-CPT9a (*21*), similar to the effects of the non-specific inhibitor, Cl-amidine, a
171 PAD4 inhibitor which also blocked the response to PMA (Fig. 3C and S3A). This revealed the RNA
172 sensor TLR8 (*22*) to be the specific naRNA receptor in primary human PMNs. We further genetically
173 validated the involvement of RNA sensing in naRNA-mediated NET propagation using BM-PMNs from
174 *Unc93b1*- or *Tlr13*-defective mice: whereas in *Unc93b1*-defective mice signaling of all endosomal
175 TLRs is abrogated (*23*), mice lacking *Tlr13,* the murine equivalent of TLR8 (*12*), specifically lack ssRNA
176 sensing (*24*). Confocal microscopy analysis showed that WT BM-PMNs responded readily to both
177 PMA (used as control) and PMA NETs, whereas *Unc93b1* (Fig. S3B) or *Tlr13* KO PMNs (Fig. 3D,
178 quantified in E) only responded to the TLR-independent PMA control but not PMA NETs. Additionally,
179 naïve BM-PMNs from *Tlr9* KO mice, which lack DNA sensing, responded to both PMA and PMA NETs
180 with NET formation just like WT BM-PMNs (Fig. S3C), emphasizing the redundancy of DNA vs the key
181 role of naRNA in the self-propagating properties of NETs. This receptor analysis unequivocally
182 confirmed naRNA to be a primary immune stimulant in NETs.

183 **PMN-derived naRNA triggers broader immune cell and keratinocyte activation**

184 Given the potent effect of naRNA on naïve PMNs (*cf.* Fig. 3B-E) and the ability of human
185 macrophages to sense RNA via TLR8 (*25*), we hypothesized that naRNA might also directly activate
186 macrophages, which are rapidly recruited at the sites of PMN activation in peripheral tissues (*26*),
187 contributing to an inflammatory process in vivo. We thus assessed the effects of naRNA on
188 genetically modified macrophage-like cell lines: BlaER1 macrophages (*27*) responded to PMA NETs
189 but not mock NETs with IL-8 release, and this was TLR8-dependent as evidenced by comparisons of
190 WT and *TLR8*-edited BlaER1 cells (Fig. 3F). Use of a naRNA-stabilizing RNase inhibitor during NET
191 preparation (*cf.* Fig. 2B) drastically increased the potency of PMA NETs on these macrophages.
192 Additionally, TLR8 and TLR7-edited THP-1 macrophage-like cells (*28*) responded to PMA NETs with
193 lower relative IL-8 release than WT THP-1 cells (Fig. S4A), confirming RNA as the active agent in
194 monocyte/macrophage activation. Human peripheral blood mononuclear cells (PBMCs) were also
195 stimulated with different NET preparations. RNA-stabilized PMA NETs consistently elicited higher

196 TNF, IL-6 and IL-8 levels than non-stabilized PMA- or mock NETs (Fig. S4B-D). However, this effect was
197 not sensitive to the TLR8 inhibitor Cu-CPT9a, which is consistent with the ability of TLR7 to also sense
198 naRNA (*cf.* Fig. 3A) and possibly due to a mixture of cells being present. Further analysis revealed that
199 the natural killer (NK) cell line NK-92 MI showed low IFNγ release in response to RNA-stabilized PMA
200 NETs (Fig. S4E). Collectively, our results show that the RNA component of NETs, naRNA, can engage
201 not only bystander neutrophils in a feed-forward inflammatory response but also other myeloid
202 (monocytes/macrophages) and lymphoid (NK cells) cellular innate immunity. To investigate whether
203 non-hematopoietic cells with immune functions, e.g. tissue cells like keratinocytes, could also
204 respond to RNA-stabilized PMA NETs, N/TERT-1 keratinocytes (*29*) in monolayers were exposed to
205 PMA-NETs (Fig. 3G). This triggered a dose-dependent IL-8 release comparable to synthetic RNA+LL37,
206 especially under RNA stabilization by RNase inhibitors. Similar results were obtained using
207 monolayers of primary normal human epidermal keratinocyte (NHEK) from healthy donors (Fig. 3H).
208 Furthermore, in an 'in vivo'-like human skin equivalent 3D model in which natural keratinocyte
209 differentiation was recapitulated by NHEK cells (*30*), PMA but not mock NETs significantly induced *IL8*
210 mRNA and protein (Fig. 3I, J). Thus, naRNA can not only activate primary neutrophils in vitro but also
211 trigger broad immune activation in other immune and tissue cells/equivalents.

212 **naRNA displays DAMP activity in vivo in dependence on RNA sensing**

213 Moreover, to gain an insight into whether naRNA could trigger inflammation in vivo in an RNA
214 receptor-dependent manner, we intradermally injected RNase inhibitor-stabilized mock or PMA NETs
215 in the ears of C57BL6 mice. RNA-stabilized PMA NETs were almost as potent to induce ear swelling as
216 synthetic RNA+LL37 (Fig. 4A), but even non-stabilized PMA NETs induced a response significantly
217 higher than mock NETs. The same stimulants were also injected into the ear of *LysM*$^{EGFP/+}$ mice, in
218 which myeloid cells are GFP-positive, thus enabling in vivo monitoring of cellular influx during skin
219 inflammation. Here, RNA-stabilized PMA NETs elicited even greater cellular influx than synthetic
220 RNA+LL37 and mock NETs (Fig. 4B). Importantly, a comparison of WT and *Tlr13*-deficient animals
221 showed that the ear swelling reaction resulting in vivo was naRNA-dependent because RNA-
222 stabilized PMA-NETs were significantly less effective in *Tlr13*-deficient animals (Fig. 4C).

223 **RNA recognition contributes to progressive skin inflammation in experimental psoriasis**

224 Finally, we sought to explore if naRNA was relevant in an animal disease model. The most frequently
225 used murine model of psoriasis uses the TLR7 ligand imiquimod (IMQ) to trigger increasing skin
226 inflammation characterized by epidermal thickening and immune cell infiltration (*31*). We previously
227 showed that IMQ treatment also leads to the occurrence of NETs in the tissue (*8*). We therefore
228 speculated that naRNA might be involved in disease progression, a hypothesis that could be probed
229 by genetically ablating naRNA sensing and comparing WT and *Tlr13* KO mice. Although in the early

230 induction phase, WT and *Tlr13* KO animals showed a similar increase in ear thickness, the groups
231 diverged from day 3 onwards, after which *Tlr13*-deficient animals were significantly protected from
232 skin inflammation compared to WT mice (Fig. 4D). Additionally, the characteristic epidermal
233 thickening upon IMQ treatment was significantly lower in *Tlr13*-deficient mice compared to WT mice
234 (Fig. 4E, representative image Fig. 4F). The most plausible explanation is that IMQ-initiated NET
235 formation (*8*) amplifies skin inflammation in WT animals via naRNA, whereas this is prevented in
236 *Tlr13* KO animals. This shows that naRNA can significantly contribute to inflammation in a well-
237 established disease model and can act as a potent inflammation-amplifying endogenous DAMP, e.g.
238 in psoriasis.

239 **naRNA and LL37 await externalization in an already pre-associated DAMP state in healthy donor**
240 **neutrophils**

241 Thus far, our data aligned well with the notion of the association of LL37 and RNA in the chaotic
242 assembly of the NET accidentally generating a composite DAMP in which LL37 would exert the
243 breaking of tolerance to self-RNA. Indeed, in confocal microscopy (Fig. 5A), Pearson's colocalization
244 analysis (Fig. 5B) and additional line plot quantification (Figs. 5C and S5) of PMA-stimulated PMN
245 NETs, RNA and LL37 did in fact co-localize in NETs, i.e., after extrusion. However, most surprisingly, in
246 unstimulated PMNs naRNA and LL37 showed even greater Pearson's colocalization (Fig. 5B) and,
247 unlike DNA, shared co-localization maxima (Fig. 5C, Fig. S5), suggesting the intriguing notion of pre-
248 association of RNA and LL37 even before extrusion. To verify this further, rRNA and LL37 double
249 staining on ultrathin (50-60 nm) sections of resting PMN confirmed the reported localization of LL37
250 to neutrophil granules (*32*), but also the unexpected concomitant presence of rRNA in the same
251 structures (Fig. 5D). Transmission electron microscopy combined with double staining of rRNA and
252 LL37 using two different immunogold sizes corroborated this further at even higher magnification
253 (Fig. 5E).The concept of pre-packaging of RNA with LL37 in specific compartments also fits with the
254 RNAseq data showing that certain RNA types are lost upon release (*cf.* Fig. 1H), probably because
255 they are not bound to LL37. Of note, the effect was seen in normal peripheral blood PMN across
256 multiple healthy donors, indicating that LL37 association with RNA is a normal physiological PMN
257 property. In turn, and in line with our initial analysis (*cf.* Fig. 1A/C), this would mean that every NET is
258 intended to contain and externalize naRNA-LL37 DAMPs.

259 ## Discussion

260 At first sight, it may not seem surprising that the release of NETs, a process that churns up the most
261 critical compartment of a cell, e.g., the nucleus, also inevitably leads to the release of another
262 primary cellular biomolecule, namely RNA. However, independently of whether the process is
263 regulated or not, the release of RNA by NETting PMNs appears to have physiological importance as

264 we have demonstrated here. Rather than acting directly in antimicrobial defense (*cf.* Fig. S2A),
265 naRNA appears to be an LL37-associated DAMP of PMN origin that can be released in the NETting
266 process, and then activates both PMN and other immune and tissue cells in an RNA sensor-
267 dependent manner (Fig. S6). Several further findings warrant further discussion:

268 Firstly, our data revise previous concepts of self-RNA and LL37 in the 'breaking' of innate immune
269 tolerance in psoriasis and the physiological role of NETs in general. naRNA when complexed with
270 LL37, gains stimulatory properties, in line with the existing notion that LL37 may 'break' immune
271 tolerance by acting as a physiological 'transfection reagent' for uptake into immune cells, and by
272 shielding it from RNase degradation. However, our data show that RNA and LL37 do aggregate and
273 co-localize 'accidentally' in the chaotic mesh of the NET: quite unexpectedly, they were rather found
274 in a kind of 'pre-association' in the same intracellular storage compartments before extrusion during
275 NET formation. It will be interesting to study the process for pre-association for this first 'composite
276 DAMP' and elucidate the precise nature of the RNAs assembled with LL37 in the future. But already
277 the identification of such pre-association challenges existing concepts of LL37-RNA complexes as
278 'accidentally assembled' tolerance breakers in certain diseases (*10*). Rather, it suggests naRNA-LL37
279 complexes act as purposefully pre-associated DAMPs that arm neutrophils at steady state and are
280 meant to 'break tolerance' and cause immune-activation in healthy donors – with other
281 pathomechanism causing chronic disease in e.g. psoriasis patients. Especially since the here-
282 described phenomena were found with neutrophils and other cells from healthy donors, intentional
283 (rather than accidental/extracellular) pre-association points to a very specific but broadly relevant
284 novel role of the naRNA-LL37 DAMP in NET biology: The fact that NETs have been described for a
285 multitude of sterile conditions, would anyways argue that antimicrobial cannot represent the
286 primary, let alone only, intended purpose of this widespread phenomenon. Rather, based our
287 findings, we believe the NET response in general to primarily be a DAMP response, calling for a re-
288 evaluation of existing concepts in NET biology. We speculate that the physiological relevance of
289 deploying this composite DAMP upon NET formation could be to tag fresh NETs with a timed
290 molecular beacon: In this scenario, freshly extruded NETs decorated with the naRNA-LL37 DAMP
291 would highlight an acute tissue insult (or the lingering presence of a pathogenic microorganism
292 during non-sterile conditions) to other cells not directly or initially engaged by the threat. The
293 naRNA-LL37 DAMP would thus label 'fresh NETs' as 'requiring attention' and trigger further immune
294 activation, clearance and eventually inflammation resolving activities. Over time, whilst the DNA-
295 related structural and antimicrobial properties of NETs may remain longer, inevitable RNA
296 degradation would lead to deactivation of the composite DAMP, rendering 'old NETs' less
297 immunostimulatory. Further work outside the scope of the present study may explore the intriguing
298 notion of naRNA as time-wise self-restricting molecular label for NETs.

299 Moreover, our data pertain to the origin and effects of 'extracellular RNA' (exRNA). exRNA is a
300 generic term to indicate a heterogeneous group of RNA molecules which are actively or passively
301 released during sterile inflammation or infectious processes. exRNA can be released in a 'free' state,
302 bound to proteins or phospholipids, in association with extracellular vesicles (EVs) or apoptotic
303 bodies (*14*). In all these forms, exRNA may function as a DAMP but also as e.g., procoagulant or
304 regenerative factor (*14*). Our data identify naRNA as the first type of exRNA for which a clearly
305 defined physiological origin/process (namely NETs) of extracellular release in physiologically relevant
306 amounts is provided. We speculate that our findings will help trace multiple descriptions of exRNA,
307 on the one side, to neutrophil traps on the other. For example, exRNA has emerged as disease-
308 relevant in atherosclerosis, where it was described to act as a proinflammatory mediator enhancing
309 the recruitment of leukocytes to the site of atherosclerotic lesions as shown in a mouse model of
310 accelerated atherosclerosis (*33*). At the same time, NETs have been ascribed a role in amplifying
311 sterile inflammatory responses in an independent mouse model of atherosclerosis by priming
312 macrophages (*3*). However, never have these two independent strains of research been connected.
313 By showing NETs to release naRNA, a DAMP type of exRNA, our work connects both lines of enquiry.
314 Likewise, for rheumatoid arthritis (RA), our work makes a plausible link between exRNA in synovial
315 fluid contributing to joint inflammation (*34*), the emerging role of NETs in RA (*4*) and even a hitherto
316 enigmatic but therapeutically relevant role of TLR8 (*35, 36*).

317 Moreover, NETs have been of broad interest focus in COVID-19-related research regarding thrombo-
318 inflammatory states, like sepsis, thrombosis, and respiratory failure, , have been found in plasma of
319 hospitalized COVID-19 patients, and linked to thrombus formation by several research groups (*37*)
320 (*38*) (*39*) (*5, 40*). Furthermore, exRNAs have been in focus as procoagulant cofactors in blood
321 coagulation (*41*) (*42*). A link between NET-related and RNA-induced thrombus formation in COVID-19
322 has never been made but highlights naRNA as a potential contributing factor of NET-induced
323 thrombo-inflammatory states in COVID-19 disease pathogenesis. Collectively, we suspect similar links
324 between NETs and exRNA via naRNA to emerge for cardiovascular diseases and cancer if the role of
325 naRNA is thoroughly assessed. Furthermore, the broad sensitivity of immune and tissue cells to
326 naRNA observed by us makes sense of how exRNA may act pathophysiologically.

327 Although we believe PMNs to be the primary trap forming human leukocyte population and hence
328 naRNA the most significant "trap-associated RNA", it will be interesting to explore whether mast cell
329 (MCETs) (*43*) or macrophage extracellular traps (METs) (*44*) contain RNA. However, unlike PMN, the
330 latter immune cells are not primary sources of LL37 (*32*), so that RNA associated with MCETs or METs
331 would be of lesser physiological relevance as a DAMP than naRNA due to a lack of LL37. Therefore,
332 translational approaches, e.g., to restrict trap-RNA mediated amplification of inflammation, should
333 probably center on PMN-derived naRNA. The use of PAD4 inhibitors has already been investigated in

334 animal models to treat cancer or atherosclerotic lesions (*45, 46*) and would represent one potential
335 way of eliminating NETs and hence naRNA-mediated inflammation. However, this would also prevent
336 the effects of NETs that are beneficial for host defense (e.g. physical trapping via DNA and
337 antimicrobial enzymatic activities) and may render treated patients vulnerable to infections. From a
338 translational perspective, our in vivo data indicate that blockade of RNA sensing might be more
339 advantageous, restricting only naRNA-mediated responses. Although probably not applicable to
340 patients, it is underscored by evidence that neuroinflammation upon subarachnoid hemorrhage,
341 which is characterized by a NET pathology, is strongly ameliorated by RNase treatment in vivo (*47*).
342 More applicable to patients may be the targeting of TLR8 by small molecular antagonists (*48*) or
343 inhibitory oligonucleotides, which are able to block PMN responsiveness to synthetic RNA in vitro (*8*).
344 Exciting is thus the observed efficacy of TLR inhibitory oligoribonucleotides in a psoriasis mouse
345 model (*49*) and even a first clinical trial in psoriasis patients (*50*). We could imagine the blockade of
346 naRNA effects via TLRs highlighted here to emerge as an effective novel strategy to target multiple
347 exRNA or NET-related inflammatory responses.

348 ## Figure legends

349 **Fig. 1**: **naRNA is a canonical component of NETs.**

350 **(A, B)** Confocal microscopy of primary human PMNs stimulated as indicated for 3 h and stained for
351 naRNA (anti-rRNA Y10b, magenta) and DNA (Hoechst 33342, white, n = 3, scale bar: 10 µm,
352 arrowheads point to selected NET strands; representative images in **A**) were quantified in **B** (each dot
353 represents one image, *p<0.05 according to one-way ANOVA). **(C)** Confocal microscopy of primary
354 murine BM-PMNs stimulated as indicated for 16 h and stained as in **A** (n = 3, representative images,
355 scale bar: 10 µm). **(D)** Confocal microscopy of primary human stem cells differentiated *in vitro*
356 with/without 100 µM 5-ethynyluridine (5-EU), click-labeled with a fluorescent dye (yellow, total
357 RNA), anti-rRNA and Hoechst 33342 as in **A** (n = 3, representative images, scale bar: 10 µm, 2 µm in
358 cropped image). **(E)** as in **A** but showing 3D image reconstruction of z-stacks (n = 3, representative
359 images, scale bar: 10 µm). **(F)** Scanning electron microscopy of human primary PMNs treated as
360 indicated and using anti-rRNA primary and immunogold (white arrow)-labeled secondary antibodies
361 and silver enhancement (n = 3, representative images, scale bars as indicated; the two rightmost
362 images show composite images with signals from secondary electron and backscattered electron
363 detectors for topography and additional material information, respectively). **(G)** Agilent TapeStation
364 quantification of naRNA isolated from mock or PMA NETs (from n = 4-6 donors, combined data,
365 mean+SD, each dot represents one biological replicate/donor, *p<0.05 according to Mann-Whitney
366 test). **(H)** RNAseq of PMA NET naRNA (n = 4) and whole PMN RNA (n = 1) (combined data).

367 **Fig. 2. naRNA is a composite DAMP driving NET propagation in human PMN**

368 **(A)** Workflow for NET content preparation from one donor and transfer to naïve human primary
369 PMNs from a second donor. **(B)** Confocal microscopy of primary human PMNs stimulated with NET
370 content harvested with/without RNase inhibitor and diluted 1:50 or 1:500, and then stained for
371 NETs/DNA (Hoechst 33342, n = 9, representative images, scale bar: 10 µm). **(C)** Quantification of **B**
372 using DNA (Hoechst 33342) signal to quantify NET formation (n = 3, combined data, mean+SD, each
373 dot represents one image, *p<0.05 according to one-way ANOVA). **(D)** as in **B** but with/without pre-
374 digestion of NET content with RNase A (n = 3, representative images, scale bar: 10 µm). **(E)**
375 Quantification of **D** (n = 3, combined data, mean+SD, each dot represents the number of NET-positive
376 tiles in one image quantified from three images/condition, *p<0.05 according to one-way ANOVA).
377 **(F)** As in **B** but using purified naRNA (*cf.* Fig. 1G) alone or in complex with exogenously added LL37 (n
378 = 3, representative images, scale bar: 10 µm).

379 **Fig. 3. naRNA activity depends on RNA sensors**

380 **(A)** NF-κB dual luciferase assay in HEK293T cell transiently transfected and stimulated as indicated
381 (eV = empty vector, n=3-5, combined data, mean+SD, *p<0.05 according to one-way ANOVA). **(B)**
382 Confocal microscopy of human primary PMNs stimulated as indicated in the presence or absence of
383 CU-CPT9a (100 nM) or Cl-amidine (200 µM, not shown) and stained for NETs/DNA (Hoechst 33342,
384 white, n = 3, representative images, scale bar: 10 µm). **(C)** Quantification of **B** using DNA (Hoechst
385 33342) signal to quantify NET formation (n = 3, combined data, mean+SD, each dot represents the
386 number of NET-positive tiles in one image, three images/condition, *p<0.05 according to non-
387 parametric one-way ANOVA). **(D)** Confocal microscopy analysis of primary C57BL/6 WT or *Tlr13*$^{-/-}$
388 murine BM-PMNs stimulated as indicated and stained for NETs/DNA (Hoechst 33342, white, n = 3,
389 representative images, scale bar: 10 µm). **(E)** Quantification of **D** as in **C** (n = 3, *p<0.05 according to
390 one-way ANOVA). **(F)** Triplicate IL-8 ELISA from WT, *TLR8*$^{-/-}$ and *UNC93B1*$^{-/-}$ BlaER1 macrophage-like
391 cells stimulated as indicated for 18 h (n = 3-4, combined data, mean+SD, each dot represents one
392 biological replicate, *p<0.05 according to one-way ANOVA). **(G)** Triplicate IL-8 ELISA from N/TERT-1
393 keratinocytes stimulated as indicated for 24 h (n = 3, combined data, mean+SD, each dot represents
394 one biological replicate, *p<0.05 according to one-way ANOVA). **(H)** As in **G** but with primary normal
395 human epidermal keratinocytes (NHEK) (n = 3, combined data, mean+SD, each dot represents one
396 biological replicate, *p<0.05 according to one-way ANOVA). **(I, J)** Triplicate relative (to unstimulated)
397 *IL8* mRNA qPCR or IL-8 ELISA from NHEK 3D human skin equivalent constructs stimulated as indicated
398 for 24 h (n = 3, representative of one biological replicate is shown, mean+SD, each dot represents
399 one technical replicate, *p<0.05 according to one-way ANOVA).

400 **Fig. 4. naRNA is a driver of NET-associated *in vivo* inflammation**

401 **(A)** Ear thickness quantified daily in WT C57BL6 mice injected intradermally in vivo on day 0 as
402 indicated (n = 5 per group, combined data, mean+SD, *p<0.05 according to two-way ANOVA). **(B)**
403 Fluorescence imaging monitored hourly in *LysM*$^{EGFP/+}$ mice injected intradermally in vivo at t=0 as
404 indicated (n = 10 per group, combined data, mean+SD, *p<0.05 according to two-way ANOVA). **(C)** As
405 in **A** but also using *Tlr13*$^{-/-}$ mice (n = 7, combined data, mean+SD, *p<0.05 according to two-way
406 ANOVA). **(D)** As in **C** but instead of intradermal injection with topical imiquimod application on day 0–
407 4 (C57BL/6 n = 8, *Tlr13*$^{-/-}$ n = 10, combined data, mean+SD, *p<0.05 according to two-way ANOVA).
408 **(E)** Measurement of epidermal thickness of H&E-stained ear skin specimens of **D** (C57BL/6 n = 8,
409 *Tlr13*$^{-/-}$ n = 10, combined data, mean+SD, *p<0.05 according to Student's *t*-test). **(F)** Histological
410 analysis of H&E-stained ear skin specimens of **E** (C57BL/6 n = 8, *Tlr13*$^{-/-}$ n = 10, representative of one
411 biological replicate is shown, scale bar: 100 µm).

412 **Fig. 5: naRNA and LL37 are pre-associated in resting neutrophils**

413 **(A)** Confocal microscopy of primary human PMNs stimulated as indicated for 3 h and stained for
414 naRNA (anti-rRNA Y10b, magenta), LL37 (anti-hLL37-DyLight550, yellow), and DNA (Hoechst 33342,
415 white, n = 3, representative images, scale bar 10 µm). **(B)** Pearson's correlation coefficient
416 (colocalization) analysis of **A** (n = 3, combined data, mean+SD, each dot represents one image, three
417 images/condition, *p<0.05 according to one-way ANOVA). **(C)** Line plot analysis of LL37, RNA and
418 DNA staining of primary human PMNs stimulated as indicated of **A** was performed using ZenBlue3
419 software (n=3, representative graph). **(D)** As in **A**/C but on ultrathin sections of unstimulated PMNs
420 (n=3, representative image, scale bar 2 µm). Line plot analysis was performed using ImageJ-Win64
421 software (n=3, representative graph). **(E)** Transmission electron microscopy of unstimulated human
422 primary PMNs using anti-rRNA and anti-hLL-37 primary and immunogold (6 nm (black arrow) and 12
423 nm (white arrow) respectively)-labeled secondary antibodies (n = 3, representative images, scale bars
424 as indicated).

425 **References**

426 1. V. Brinkmann *et al.*, Neutrophil extracellular traps kill bacteria. *Science* **303**, 1532-1535
427 (2004).
428 2. P. Kruger *et al.*, Neutrophils: Between host defence, immune modulation, and tissue injury.
429 *PLoS Pathog* **11**, e1004651 (2015).
430 3. A. Warnatsch, M. Ioannou, Q. Wang, V. Papayannopoulos, Inflammation. Neutrophil
431 extracellular traps license macrophages for cytokine production in atherosclerosis. *Science*
432 **349**, 316-320 (2015).
433 4. W. Song, J. Ye, N. Pan, C. Tan, M. Herrmann, Neutrophil Extracellular Traps Tied to
434 Rheumatoid Arthritis: Points to Ponder. *Front Immunol* **11**, 578129 (2020).
435 5. B. J. Barnes *et al.*, Targeting potential drivers of COVID-19: Neutrophil extracellular traps. *J*
436 *Exp Med* **217**, (2020).
437 6. S. Boeltz *et al.*, To NET or not to NET:current opinions and state of the science regarding the
438 formation of neutrophil extracellular traps. *Cell Death Differ* **26**, 395-408 (2019).
439 7. B. Altincicek, S. Stotzel, M. Wygrecka, K. T. Preissner, A. Vilcinskas, Host-derived extracellular
440 nucleic acids enhance innate immune responses, induce coagulation, and prolong survival
441 upon infection in insects. *J Immunol* **181**, 2705-2712 (2008).
442 8. F. Herster *et al.*, Neutrophil extracellular trap-associated RNA and LL37 enable self-amplifying
443 inflammation in psoriasis. *Nat Commun* **11**, 105 (2020).
444 9. R. Lande *et al.*, Plasmacytoid dendritic cells sense self-DNA coupled with antimicrobial
445 peptide. *Nature* **449**, 564-569 (2007).
446 10. D. Ganguly *et al.*, Self-RNA-antimicrobial peptide complexes activate human dendritic cells
447 through TLR7 and TLR8. *J Exp Med* **206**, 1983-1994 (2009).
448 11. R. Lande *et al.*, Cationic antimicrobial peptides in psoriatic skin cooperate to break innate
449 tolerance to self-DNA. *Eur J Immunol* **45**, 203-213 (2015).
450 12. T. Eigenbrod, A. H. Dalpke, Bacterial RNA: An Underestimated Stimulus for Innate Immune
451 Responses. *J Immunol* **195**, 411-418 (2015).
452 13. N. A. Lind, V. E. Rael, K. Pestal, B. Liu, G. M. Barton, Regulation of the nucleic acid-sensing
453 Toll-like receptors. *Nat Rev Immunol* **22**, 224-235 (2022).
454 14. K. T. Preissner, S. Fischer, E. Deindl, Extracellular RNA as a Versatile DAMP and Alarm Signal
455 That Influences Leukocyte Recruitment in Inflammation and Infection. *Front Cell Dev Biol* **8**,
456 619221 (2020).
457 15. B. Schmidt *et al.*, Quantification of free RNA in serum and bronchial lavage: a new diagnostic
458 tool in lung cancer detection? *Lung Cancer* **48**, 145-147 (2005).
459 16. A. Zernecke, K. T. Preissner, Extracellular Ribonucleic Acids (RNA) Enter the Stage in
460 Cardiovascular Disease. *Circ Res* **118**, 469-479 (2016).
461 17. E. A. Lerner, M. R. Lerner, C. A. Janeway, Jr., J. A. Steitz, Monoclonal antibodies to nucleic
462 acid-containing cellular constituents: probes for molecular biology and autoimmune disease.
463 *Proc Natl Acad Sci U S A* **78**, 2737-2741 (1981).
464 18. S. I. Presolski, V. P. Hong, M. G. Finn, Copper-Catalyzed Azide-Alkyne Click Chemistry for
465 Bioconjugation. *Curr Protoc Chem Biol* **3**, 153-162 (2011).
466 19. M. Sioud, RNA Interference and CRISPR Technologies Technical Advances and New
467 Therapeutic Opportunities Preface. *Methods Mol Biol* **2115**, V-Vii (2020).
468 20. E. Colak *et al.*, RNA and imidazoquinolines are sensed by distinct TLR7/8 ectodomain sites
469 resulting in functionally disparate signaling events. *J Immunol* **192**, 5963-5973 (2014).
470 21. S. Zhang *et al.*, Small-molecule inhibition of TLR8 through stabilization of its resting state. *Nat*
471 *Chem Biol* **14**, 58-64 (2018).
472 22. F. Heil *et al.*, Species-specific recognition of single-stranded RNA via toll-like receptor 7 and 8.
473 *Science* **303**, 1526-1529 (2004).
474 23. K. Tabeta *et al.*, The Unc93b1 mutation 3d disrupts exogenous antigen presentation and
475 signaling via Toll-like receptors 3, 7 and 9. *Nat Immunol* **7**, 156-164 (2006).

476 24. X. D. Li, Z. J. Chen, Sequence specific detection of bacterial 23S ribosomal RNA by TLR13. *Elife*
477 **1**, e00102 (2012).
478 25. N. Ishii, K. Funami, M. Tatematsu, T. Seya, M. Matsumoto, Endosomal localization of TLR8
479 confers distinctive proteolytic processing on human myeloid cells. *J Immunol* **193**, 5118-5128
480 (2014).
481 26. B. Mahdavian Delavary, W. M. van der Veer, M. van Egmond, F. B. Niessen, R. H. Beelen,
482 Macrophages in skin injury and repair. *Immunobiology* **216**, 753-762 (2011).
483 27. T. Vierbuchen, C. Bang, H. Rosigkeit, R. A. Schmitz, H. Heine, The Human-Associated
484 Archaeon Methanosphaera stadtmanae Is Recognized through Its RNA and Induces TLR8-
485 Dependent NLRP3 Inflammasome Activation. *Front Immunol* **8**, 1535 (2017).
486 28. C. Coch *et al.*, Human TLR8 Senses RNA From Plasmodium falciparum-Infected Red Blood
487 Cells Which Is Uniquely Required for the IFN-gamma Response in NK Cells. *Front Immunol* **10**,
488 371 (2019).
489 29. M. A. Dickson *et al.*, Human keratinocytes that express hTERT and also bypass a p16(INK4a)-
490 enforced mechanism that limits life span become immortal yet retain normal growth and
491 differentiation characteristics. *Mol Cell Biol* **20**, 1436-1447 (2000).
492 30. K. Bitschar *et al.*, Lugdunin amplifies innate immune responses in the skin in synergy with
493 host- and microbiota-derived factors. *Nat Commun* **10**, 2730 (2019).
494 31. M. Gilliet *et al.*, Psoriasis triggered by toll-like receptor 7 agonist imiquimod in the presence
495 of dermal plasmacytoid dendritic cell precursors. *Arch Dermatol* **140**, 1490-1495 (2004).
496 32. O. Sorensen, K. Arnljots, J. B. Cowland, D. F. Bainton, N. Borregaard, The human antibacterial
497 cathelicidin, hCAP-18, is synthesized in myelocytes and metamyelocytes and localized to
498 specific granules in neutrophils. *Blood* **90**, 2796-2803 (1997).
499 33. S. Simsekyilmaz *et al.*, Role of extracellular RNA in atherosclerotic plaque formation in mice.
500 *Circulation* **129**, 598-606 (2014).
501 34. E. Neumann, R. Hasseli, U. Lange, U. Muller-Ladner, The Role of Extracellular Nucleic Acids in
502 Rheumatoid Arthritis. *Curr Pharm Biotechnol* **19**, 1182-1188 (2018).
503 35. S. Sacre *et al.*, Oligodeoxynucleotide inhibition of Toll-like receptors 3, 7, 8, and 9 suppresses
504 cytokine production in a human rheumatoid arthritis model. *Eur J Immunol* **46**, 772-781
505 (2016).
506 36. S. M. Sacre *et al.*, Inhibitors of TLR8 reduce TNF production from human rheumatoid synovial
507 membrane cultures. *J Immunol* **181**, 8002-8009 (2008).
508 37. Y. Zuo *et al.*, Neutrophil extracellular traps in COVID-19. *JCI Insight* **5**, (2020).
509 38. A. Yaqinuddin, J. Kashir, Novel therapeutic targets for SARS-CoV-2-induced acute lung injury:
510 Targeting a potential IL-1beta/neutrophil extracellular traps feedback loop. *Med Hypotheses*
511 **143**, 109906 (2020).
512 39. S. Cicco, G. Cicco, V. Racanelli, A. Vacca, Neutrophil Extracellular Traps (NETs) and Damage-
513 Associated Molecular Patterns (DAMPs): Two Potential Targets for COVID-19 Treatment.
514 *Mediators Inflamm* **2020**, 7527953 (2020).
515 40. R. M. Golonka *et al.*, Harnessing innate immunity to eliminate SARS-CoV-2 and ameliorate
516 COVID-19 disease. *Physiol Genomics* **52**, 217-221 (2020).
517 41. C. Kannemeier *et al.*, Extracellular RNA constitutes a natural procoagulant cofactor in blood
518 coagulation. *Proc Natl Acad Sci U S A* **104**, 6388-6393 (2007).
519 42. A. Sahu *et al.*, MicroRNA-145 Impedes Thrombus Formation via Targeting Tissue Factor in
520 Venous Thrombosis. *EBioMedicine* **26**, 175-186 (2017).
521 43. H. Mollerherm, M. von Kockritz-Blickwede, K. Branitzki-Heinemann, Antimicrobial Activity of
522 Mast Cells: Role and Relevance of Extracellular DNA Traps. *Front Immunol* **7**, 265 (2016).
523 44. R. S. Doster, L. M. Rogers, J. A. Gaddy, D. M. Aronoff, Macrophage Extracellular Traps: A
524 Scoping Review. *J Innate Immun* **10**, 3-13 (2018).
525 45. M. Li *et al.*, A Novel Peptidylarginine Deiminase 4 (PAD4) Inhibitor BMS-P5 Blocks Formation
526 of Neutrophil Extracellular Traps and Delays Progression of Multiple Myeloma. *Mol Cancer*
527 *Ther* **19**, 1530-1538 (2020).

528 46. J. S. Knight *et al.*, Peptidylarginine deiminase inhibition reduces vascular damage and
529 modulates innate immune responses in murine models of atherosclerosis. *Circ Res* **114**, 947-
530 956 (2014).
531 47. A. Fruh *et al.*, RNase A Inhibits Formation of Neutrophil Extracellular Traps in Subarachnoid
532 Hemorrhage. *Front Physiol* **12**, 724611 (2021).
533 48. J. Vlach *et al.*, Discovery of M5049: A Novel Selective Toll-Like Receptor 7/8 Inhibitor for
534 Treatment of Autoimmunity. *J Pharmacol Exp Ther* **376**, 397-409 (2021).
535 49. W. Jiang *et al.*, A Toll-like receptor 7, 8, and 9 antagonist inhibits Th1 and Th17 responses and
536 inflammasome activation in a model of IL-23-induced psoriasis. *J Invest Dermatol* **133**, 1777-
537 1784 (2013).
538 50. D. M. Balak *et al.*, IMO-8400, a toll-like receptor 7, 8, and 9 antagonist, demonstrates clinical
539 activity in a phase 2a, randomized, placebo-controlled trial in patients with moderate-to-
540 severe plaque psoriasis. *Clin Immunol* **174**, 63-72 (2017).
541 51. T.-H. Chang *et al.*, Transkingdom mechanism of MAMP generation by chitotriosidase (CHIT1)
542 feeds oligomeric chitin from fungal pathogens and allergens into TLR2-mediated innate
543 immune sensing. *bioRxiv*, 2022.2002.2017.479713 (2022).
544 52. N. Faust, F. Varas, L. M. Kelly, S. Heck, T. Graf, Insertion of enhanced green fluorescent
545 protein into the lysozyme gene creates mice with green fluorescent granulocytes and
546 macrophages. *Blood* **96**, 719-726 (2000).
547 53. K. Bitschar *et al.*, Staphylococcus aureus Skin Colonization Is Enhanced by the Interaction of
548 Neutrophil Extracellular Traps with Keratinocytes. *J Invest Dermatol* **140**, 1054-1065 e1054
549 (2020).
550 54. G. W. Zack, W. E. Rogers, S. A. Latt, Automatic-Measurement of Sister Chromatid Exchange
551 Frequency. *J Histochem Cytochem* **25**, 741-753 (1977).
552

553 ## Additional information

554 **Author contributions:** according to Credit guidelines:

	FB	CGL	CY	SC	YW	MN	JF	JS	PE	MD	KH	BS	SB	MWL	YS	NKA	ANRW
Conceptualization	x																x
Data curation																	
Formal analysis	x	x	x	x		x	x	x	x		x					x	x
Funding acquisition												x					x
Investigation	x	x	x	x		x	x	x	x	x	X						
Methodology											X				x		
Project administration					x									X			
Resources													x	X			
Software																	
Supervision	X											x			x	x	x
Validation	X															x	x
Visualization	x	x	x								X						
Writing: original draft	x																X
Writing: review and editing	x	x	x	x	x	x	x	x	x	x	x	x	x	x	x	x	x

555 **Conflict of interest statement**

556 NKA has received previous grant support from Pfizer and Boehringer Ingelheim and was a paid
557 consultant for Janssen Pharmaceuticals. All other authors declare no competing interests. S.D.G.

558 **Acknowledgments**

559 We gratefully acknowledge Jim Rheinwald, Holger Heine, Austin Chang, Thomas Zillinger for the
560 provision of reagents, respectively, and Jon Kagan, Alexander Dalpke and Libera Lo Presti for helpful
561 scientific and editorial comments. We further acknowledge Bettina Danker, Mark Helm and Martina
562 Christina Schmidt-Dengler for very helpful technical and scientific support. We thank all voluntary
563 healthy donors of biomaterials for participating in the study. The study was supported by the
564 Deutsche Forschungsgemeinschaft (German Research Foundation, DFG) grants CRC TR156 "The skin
565 as an immune sensor and effector organ – Orchestrating local and systemic immunity" (to FB, CG, JF,
566 JS, BS and ANRW), NIH grants R01AI146177, R01AR073665, and R01AR069502 (to NKA). NKA. has
567 received previous grant support from Pfizer and Boehringer Ingelheim and was a paid consultant for
568 Janssen Pharmaceuticals. Infrastructural funding was provided by the University of Tübingen, the
569 University Hospital Tübingen and the DFG Clusters of Excellence "iFIT – Image-Guided and
570 Functionally Instructed Tumor Therapies" (EXC 2180, to AW, PE, BS and MWL), "CMFI – Controlling
571 Microbes to Fight Infection (EXC 2124 to AW and BS). Gefördert durch die Deutsche
572 Forschungsgemeinschaft (DFG) im Rahmen der Exzellenzstrategie des Bundes und der Länder - EXC
573 2180 and EXC 2124. The authors declare no competing financial interests.

574

575 ## Abbreviations

576 AF – Alexa Fluor; bRNA – bacterial ribonucleic acid; DAMP – damage-associated molecular pattern; 5-
577 EU – 5-Ethynyluridine; FACS – Fluorescence Activated Cell Sorting; fRNA – fungal ribonucleic acid;
578 H&E - Hematoxylin and Eosin; HEK – Human embryonic kidney; HMGB-1 – High-Mobility-Group-
579 Protein B1; HSC – hematopoietic stem cell; IFN – Interferon; IL – Interleukin; KO – knockout; MCET –
580 Mast cell extracellular trap; MET – Macrophage extracellular trap; MPO – Myeloperoxidase; naRNA –
581 Neutrophil extracellular trap-associated RNA; NET – Neutrophil extracellular trap; NK – natural killer;
582 PAD4 - Peptidyl arginine deiminase 4; PBMC - Peripheral Blood Mononuclear Cell; PKC- Protein kinase
583 C; PMN – Polymorphonuclear leukocytes; RT – room temperature; SEM – scanning electron
584 microscopy; TLR – Toll-like receptor; TNF – Tumor necrosis factor

585 ## Full online materials and methods

586 **Reagents**

587 PMA (tlrl-pma), Nigericin (tlrl-nig), LL37 (tlrl-l37), as well as the PRR ligands LPS (tlrl-peklps), R848
588 (tlrl-r848), TL8 (tlrl-tl8506), and the TLR8-inhibitor CU-CPT9a (inh-cc9a) were from Invivogen,
589 Ionomycin was acquired from Sigma (I0634-1MG). RNase inhibitor (N2615) was from Promega,
590 RNase A (EN0531), DNase I (EN0521) and DNase inhibitor (EN0521) were from Thermo Fisher. The
591 PAD4-inhibitor Cl-amidine (506282) was from Merck Millipore. DOTAP (L787.2) was from Roth (see
592 Supplementary Table S1), ssRNA40 was from Eurogentec and CpG PTO 2006 from TIB Molbiol (see
593 Supplementary Table S2). Bacterial RNA isolated from *S. aureus* was prepared as described (*8*).
594 Fungal RNA from *C. albicans* strain SC5314 was isolated as described below, as well as naRNA
595 isolated from PMA NETs. For complex formation to stimulate cells in a volume of 500 µL, 5.8 µM
596 ssRNA40 (~ 34.4 µg/mL), fungal RNA (125 ng/mL), bacterial RNA (10 µg/mL) or PMA NET derived
597 naRNA (~ 600 ng/mL) was mixed with 10 µg LL37 and left for 1 h at room temperature (RT). For a
598 smaller volume of cells, complexes were used in the according fractional amount. For RNA-only or
599 LL37-only controls, the same amounts and volumes were used replacing one of the components with
600 sterile, endotoxin-free H_2O. For complex formation with DOTAP, the according RNA or CpG was
601 incubated with the transfection reagent for 10 min at RT prior to stimulation of the cells. NET content
602 for stimulation was prepared as described below. Antibodies used for fluorescence microscopy, as
603 well as click chemistry reagents are listed in Supplementary Tables S3 and S4. Constructs used for
604 transfection of HEK293T cells are listed in Supplementary Table S5.

605 **Preparation of fungal RNA from *C. albicans***

606 *C. albicans* SC5314 (kindly cultured and prepared by Tzu-Hsuan Chang, Tübingen) was plated in a
607 slant tube containing YPD agar and grown overnight at 30 °C as described in (*51*). One colony was
608 picked from the slant tube and resuspended in 500 µL YPD medium, centrifuged at 10,000 rpm for 1
609 min and washed with phosphate-buffered saline (PBS). Afterwards, the pellet was resuspended in
610 200 µL RLT buffer (derived from RNeasy Mini Kit, Qiagen, #74106) and transferred into a 2 mL tube
611 containing 0.5 mm diameter ceramic beads. The tube was filled up to 1 mL with RLT buffer and the
612 fungi were subsequently homogenized by using a microtube homogenizer (BeadBug™, Merck) with
613 an interval of seven times 2 min shaking at 2800 rpm and 1 min cooling break on ice. The
614 supernatant was transferred into a new tube containing 1 mL 75% ethanol (VWR, 20821.330). The
615 further RNA isolation was performed according to the manufacturer's instructions using the Qiagen
616 RNeasy Mini Kit for purification of Total RNA from Animal Tissues (RNeasy Mini Kit, Qiagen, 74106).
617 The RNA was eluted in 30 µL RNase DNase-free H_2O and the concentration was determined with a
618 Nanodrop Spectrophotometer.

619 **Mice**

620 *Unc93b1*$^{3d/3d}$ (*23*), *Tlr13*$^{-/-}$ (*24*) (both kindly provided by Tatjana Eigenbrod, Heidelberg and on
621 C57BL/6 background) and WT C57BL/6 mice between 8 and 20 weeks of age were used in
622 accordance with local institutional guidelines on animal experiments, regular hygiene monitoring,
623 and specific locally approved protocols compliant with the German regulations of the Gesellschaft für
624 Versuchstierkunde/Society for Laboratory Animal Science (GV-SOLAS) and the European Health Law
625 of the Federation of Laboratory Animal Science Associations (FELASA) for sacrificing and *in vivo* work.
626 *Unc93b1*$^{3d/3d}$, *Tlr13*$^{-/-}$ and WT C57BL/6 control mice were housed in controlled specific-pathogen-free
627 animal facilities at the Interfaculty Institute of Cell Biology, Tübingen. Local federal authority for the
628 approval of experimental protocols was the Regierungspräsidium Tübingen. *Tlr9*$^{-/-}$ mice and matched
629 WT C57BL/6 control mice were a kind gift from Birgit Schittek, Tübingen. LysM$^{EGFP/+}$ [52](*52*)(*52*), *Tlr13*$^{-/-}$
630 mice (*24*) (kindly provided by James Chen, Houston and David Nemazee, La Jolla) and WT (all on a
631 C57BL/6 background) mouse strains were bred and maintained under the specific pathogen-free
632 conditions, with air isolated cages at an American Association for the Accreditation of Laboratory

633 Animal Care (AAALAC)-accredited animal facility at Johns Hopkins University and handled according
634 to procedures described in the Guide for the Care and Use of Laboratory Animals as well as Johns
635 Hopkins University's policies and procedures as set forth in the Johns Hopkins University Animal Care
636 and Use Training Manual, and all animal experiments were approved by the Johns Hopkins University
637 Animal Care and Use Committee (MO21M378). Gender-and age-matched 6–8-week-old mice were
638 used for each experiment.

639 **Isolation and stimulation of primary bone-marrow-derived polymorphonuclear neutrophils (BM-**
640 **PMNs)**

641 Bone-marrow (BM)-PMNs were isolated from the bone marrow as described (*8*). In brief, bones were
642 isolated from the respective mice and the bone marrow was flushed out. Afterwards, neutrophils
643 were isolated using magnetic separation (mouse Neutrophil isolation kit, Miltenyi Biotec, 130-097-
644 658) following the manufacturer's instructions. In total, 1×10^5 cells/well PMNs were seeded in a
645 24-well plate, and stimulation was carried out with PMA (600 nM), ssRNA+LL37 complex (as
646 previously described), nigericin (50 µM), live *C. albicans* (MOI1) or human NET content (mock control
647 and PMA NETs, 1:50 dilution) for 16 h at 37°C and 5% CO2. Subsequently, cells were stained for
648 immunofluorescence.

649 **Study participants and human blood or tissue sample acquisition**

650 All healthy donors included in this study provided their written informed consent before
651 participation. Approval for use of biomaterials was obtained for this project by the local ethics
652 committee of the Medical Faculty Tübingen in accordance with the principles laid down in the
653 Declaration of Helsinki as well as applicable laws and regulations.

654 **Primary human neutrophil isolation and stimulation**

655 Neutrophils of healthy human donors were isolated as described (*8*). In brief, EDTA-anticoagulated
656 whole blood was diluted in PBS (Thermo Fisher, 14190-169), loaded on Ficoll (1.077 g/mL, Sigma,
657 10771) and centrifuged for 25 min at 509 x g at RT without brake. Afterwards, all layers except the
658 erythrocyte-granulocyte layer were discarded and erythrocyte lysis was performed twice (for 20 and
659 for 10 min) using 1x ammonium chloride erythrocyte lysis buffer (see Supplementary Table S6) at 4
660 °C on roller shaker. The remaining cells were resuspended in culture medium (RPMI culture medium
661 (Sigma-Aldrich, R8758) + 10% FBS (heat-inactivated, sterile filtered, Th. Geyer, 11682258)) to a
662 concentration of 1.6 x 10^6 cells/mL. 500 µL of cells were seeded in a 24-well plate for
663 immunofluorescence microscopy or 8 mL of 5 x 10^6 cells/mL in 10 cm uncoated dishes for NET
664 preparation and naRNA isolation/isolation of whole PMN RNA. After seeding, the cells were rested
665 for 30 min at 37°C and 5% CO_2, followed by 3 h stimulation with PMA (600 nM), nigericin (50 µM),
666 live *C. albicans* (MOI2), RNA+LL37 complexes (as previously described) or NET content at indicated
667 dilutions for IF or 4 h stimulation with PMA (600 nM) for NET preparation. Where indicated, the cells
668 were incubated with 100 nM TLR8-inhibitor CU-CPT9a or 200 µM PAD4-inhibitor Cl-amidine 30 min
669 before stimulation and medium was not replaced during incubation with the respective stimuli.

670 **Primary peripheral blood mononuclear cell (PBMC) isolation and stimulation**

671 PBMCs were isolated from whole blood or buffy coats as described (*8*). In brief, EDTA-anticoagulated
672 blood was diluted in PBS and density gradient separation was performed as described above. The
673 PBMC layer was then carefully transferred into another reaction tube and diluted in PBS (1:1). The
674 cell suspension was spun down at 645 × g for 8 min and the cells were washed two more times in
675 PBS and resuspended in culture medium (RPMI + 10% FBS (heat inactivated) +1% L-glutamine) at a
676 density of 1 x 10^6 cells/mL. Afterwards, 200 µL of PBMCs were seeded in a 96-well plate and
677 stimulated with LPS (100 ng/mL), R848 (5 µg/mL), TL8 (100 ng/mL), ssRNA (1.6 µg/mL) + DOTAP (50
678 µg/mL), ssRNA+LL37 complex (as described above), and respective NET content (1:20 dilution) for 24
679 h at 37°C and 5% CO_2. Where indicated, the TLR8 inhibitor CU-CPT9a was added to the cells at a
680 concentration of 1 µM 2 h before stimulation and was not removed for the incubation of the cells

681 with the respective stimuli. After the stimulation, the plate was centrifuged for 5 min at 1500 rpm
682 and the supernatant was collected and stored at -80 °C until the ELISA was performed.

683 **Preparation of NETs and isolation of naRNA/whole PMN RNA**

684 NETs were prepared by 600 nM PMA treatment for 4 h at 37°C and 5% CO_2, or cells were left
685 untreated during the incubation as the mock control. After incubation, the neutrophils were gently
686 washed three times with PBS to get rid of PMA as the stimulus for NET formation, any cytokines
687 released by the cells and unstimulated PMNs, as those do not adhere to the uncoated petri dish used
688 here. In some conditions (as indicated) during the NET preparation process and for storage, naRNA
689 was protected by addition of 10 U/µL RNase inhibitor (= mock or PMA NETs + RNase Inhibitor). For
690 digest of NETs, the NET content was incubated for 20 min at 37 °C with RNase A (Thermo Fisher,
691 EN0531; 100 µg/mL, EDTA for DNase inhibition added) at 37 °C. For isolation of naRNA, RNase
692 inhibitor was added to the PMNs during NET formation. After the above-described washing process,
693 PMA or mock NETs were resuspended in 300 µL of ML buffer and RNA isolation was performed
694 according to the manufacturer's instructions (NucleoSpin miRNA isolation kit, Macherey-Nagel,
695 740971.50). The RNA was eluted in 50 µL RNase DNase-free H_2O and the concentration was
696 determined with a Nanodrop Spectrophotometer. For isolation of whole PMN RNA, untreated PMNs
697 were directly lysed, and the RNA was isolated from the cells according to the manufacturer's
698 instructions.

699 **Preparation of human primary stem cell-derived PMNs**

700 Stem cells derived from human healthy donors were prepared and differentiated as described (*19*).
701 In brief, bone marrow was diluted in PBS, carefully layered on Ficoll-Paque medium (density: 1.077
702 g/mL) and centrifuged at 500 x g for 25 min at RT without brakes. The interphase layer containing the
703 mononuclear cell fraction was transferred to a new tube and washed twice with 30 mL ice-cold PBS
704 by centrifugation at 300 x g for 8 min at 8 °C. Further, the cells were resuspended, counted, and
705 isolated using Human CD34 MicroBead Kit (Miltenyi) for magnetic beads-based isolation of $CD34^+$
706 cells from BM-MNCs. Afterwards, the number of $CD34^+$ HPSCs was determined and cultured in $CD34^+$
707 culture medium (Stemline II Hematopoietic Stem Cell Expansion medium supplemented with 10%
708 FCS, 1% L-glutamine, 1% penicillin/streptomycin, and a human recombinant cytokine cocktail
709 consisting of 20 ng/mL IL-3, 20 ng/mL IL-6, 20 ng/mL TPO, 50 ng/mL SCF, and 50 ng/mL FLT-3L) at a
710 density of 2 x 10^5/mL at 37 °C and 5% CO_2. The medium was replaced every second day and the cells
711 were cultured for 14 days. During the differentiation process, the cells were treated with 100 µM 5-
712 ethynyluridine for 14 days for subsequent click chemistry labeling of endogenous RNA or were left
713 untreated as negative controls. To verify differentiation, cell morphology was assessed using
714 Cytospin assay. In brief, the Cytoclip™ slide clips were loaded by fitting the filter card, the sample
715 chamber, and the glass slide. An assemble Cytoclip™ slide clip was then placed in the slide clip
716 support plate of the cytospin centrifuge. 2 x 10^4 cells from liquid culture differentiation were
717 pipetted into Cytofunnel™ and centrifuged for 3 min at 200 x g. The cytospin slides were stained for 5
718 min in May-Grünwald stain, rinsed shortly with ddH_2O, and then stained for 10 min in Wright-Giemsa
719 stain. Afterwards, the slides were rinsed shortly with ddH_2O, and cell morphology was determined
720 using a microscope. To further verify differentiation, flow cytometric analysis was performed using
721 antibodies specific for the following hematopoietic/myeloid markers: CD45 (leukocyte marker), CD34
722 (HSPC marker), CD33 (promyelocyte marker), CD11b (myeloid cell marker), CD14 (monocyte marker),
723 and CD15 and CD16 (neutrophil markers). Neutrophil percentage was determined by gating on
724 neutrophils as follows: $CD45^+CD11b^+CD15^+$, or $CD45^+CD11b^+CD16^+$, or $CD45^+CD15^+CD16^+$ cells

725 **BlaER1 cell culture, transdifferentiation and stimulation**

726 BlaER1 cells (WT, *Unc93b*$^{-/-}$ and *Tlr8*$^{-/-}$), a kind gift of Holger Heine, Borstel, Germany (*27*), were
727 cultured, transdifferentiated, and stimulated for 18 h with the respective stimuli as described (*8*). In
728 brief, 1 x 10^6 cells/well were seeded in a 6-well plate and differentiated with 10 ng/mL hIL-3, 10
729 ng/mL hMCSF and 150 nM β-estradiol in complete RPMI-1640 (PANBiotech, P04-18525) for 7 days.
730 Afterwards 5 x 10^4 differentiated cells were reseeded in a 96-well plate, followed by 1 h resting. Cells

731 were treated with the respective stimuli (LPS at 0.1 µg/mL, R848 at 5 µg/mL, TL8 at 100 ng/mL or
732 ssRNA+LL37 complex as described above) and mock or PMA NETs with or without RNase inhibitor) in
733 complete medium in a total volume of 125 µL/well for 18 h. After stimulation, the cells were
734 centrifuged for 5 min at 1200 rpm, the supernatant was transferred into a new plate and stored at -
735 80°C until the ELISA was performed.

736 **THP-1 cell culture, differentiation and stimulation**

737 THP-1 cells (THP-1 cells were a kind gift from Thomas Zillinger, Bonn, Germany (*28*)), were cultured in
738 complete RPMI-1640 (Sigma, R8758-24X500ML) medium. For differentiation into macrophage-like
739 cells, 5 x 10^4 cells/well were seeded in a 96-well plate, treated with 300 ng/mL PMA and incubated
740 for 16 h at 37°C and 5% CO_2. The next day, the cells were washed three times with PBS and fresh
741 medium was added, followed by 48 h of resting. Subsequently, the medium was removed, exchanged
742 by medium containing 200 U/mL IFN-γ (Sigma, I-3265), and the cells were incubated for 6 h. After
743 repeated washing and medium exchange, cells were treated with the respective stimuli (PMA (25
744 µg/mL) + Ionomycin (0.375 µg/mL), LPS (0.1 µg/mL), R848 (5 µg/mL), TL8 (40 ng/mL), ssRNA+LL37
745 complex (as described above), mock NETs + RNase inhibitor (1:50 dilution), PMA NETs (1:50 dilution)
746 and PMA NETs + RNase inhibitor (1:50 dilution)) in complete medium in a total volume of 125 µL/well
747 for 18 h. After stimulation, the cells were centrifuged for 5 min at 1200 rpm, the supernatant was
748 transferred into a new plate and stored at -80°C until the ELISA was performed.

749 **N/TERT-1 keratinocyte cell culture and stimulation**

750 N/TERT-1 cells (a kind gift from Prof. James Rheinwald (*29*)) were cultured for less than ten passages
751 in complete CnT-07 medium (CELLnTEC, CnT-07). Two days prior to stimulation, a total amount of 2 x
752 10^4 cells/well was seeded in a 96-well plate and incubated at 37°C and 5% CO_2. The medium was
753 renewed, and the cells were stimulated in a total volume of 125 µL/well of the respective stimuli
754 diluted in medium (PMA (25 µg/mL) + Ionomycin (0.375 µg/mL), TL8 (200 ng/mL), ssRNA+LL37
755 complex (as previously described), as well as mock and PMA NETs with and without RNase inhibitor
756 at indicated dilutions). After 24 h stimulation, the cells were centrifuged at 1200 rpm for 5 min and
757 the supernatant was stored in a new plate at -80°C until further usage.

758 **Primary normal human epidermal keratinocyte (NHEK) cell culture and stimulation**

759 NHEK cells (Normal Human Epidermal Keratinocytes (NHEK) single juvenile donor, proliferating,
760 PromoCell, C-12002) were grown and stimulated in Keratinocyte Growth Medium 2 (PromoCell, C-
761 20111). Two days prior to stimulation, a total amount of 2 x 10^4 cells/well was seeded in a 96-well
762 plate and incubated at 37°C and 5% CO_2. For stimulation, the medium was renewed with basal
763 medium (PromoCell, C-20211) containing 1.7 mM $CaCl_2$ (Roth, CN93.1) and stimuli were added and
764 diluted in medium in a final volume of 125 µL (R848 (20 µg/mL), TL8 (200 ng/mL), ssRNA+LL37
765 complex, as well as mock NETs + RNase inhibitor (1:25 dilution) and PMA NETs with and without
766 RNase inhibitor (1:25 dilution)). After 24 h stimulation, the cells were centrifuged at 1200 rpm for 5
767 min and the supernatant was stored in a new plate at -80°C until further usage.

768 **Preparation of 3D human skin equivalent**

769 The 3D human skin equivalent was prepared as described (*53*). Briefly, primary fibroblasts were
770 seeded on collagen and incubated in FF medium for five days. Subsequently, primary keratinocytes
771 were added to the wells and airlifting was performed on day 12. On day 22, the 3D skin model was
772 stimulated with NET content (25 µL/well for one 3D construct grown in a 12-well chamber) or
773 respective water control for 24 h. Afterwards, supernatant was harvested for ELISA, RNA was isolated
774 for qPCR analysis and H&E staining was performed.

775 **NK-92 MI cell culture and stimulation**

776 NK-92 MI cells (kindly provided by Melanie Märklin, University Hospital Tübingen) were cultured in
777 IMDM-Medium (Lonza, 12-722F). For stimulation, a total amount of 1 x 10^5 cells/well were seeded in
778 a volume of 200 µL and rested for 2 h at 37°C and 5% CO_2. The cells were stimulated with LPS (100

779 ng/mL), CpG (2.5 µM) + DOTAP (25 µg/mL), R848 (5 µg/mL), TL8 (100 ng/mL), ssRNA (1.6 µg/mL) +
780 DOTAP (50 µg/mL), ssRNA+LL37 complex (as described above), or NET content (1:100 dilution) for 24
781 h and afterwards centrifuged for 5 min at 1500 rpm. Subsequently, the supernatant was transferred
782 into a new plate and stored at -80°C until further usage.

783 **Flow cytometry**

784 After PMN isolation, the purity and activation status of the cells was determined by flow cytometry
785 as described (*8*). In brief, 200 µL of cells were transferred into a 96-well plate (U-bottom) and
786 centrifuged for 5 min at 448 x g. Afterwards, blocking was performed using pooled human serum
787 diluted 1:10 in PBS for 15 min at 4°C. After washing, the samples were stained for 20 min at RT in
788 the dark and fixed (4% PFA in PBS) after repeated washing for 10 min at RT in the dark. After an
789 additional washing step, the cell pellets were resuspended in 300 µL PBS and measurements were
790 performed on a FACS Canto II (BD Bioscience, Diva software). Analysis was performed using FlowJo
791 V10 analysis software.

792 **RNA sequencing analysis of naRNA**

793 Isolated naRNA was analyzed for quality control using the Agilent 4200 TapeStation system.
794 Subsequently, the RNA was sequenced according to NEBNext® Ultra™ II Directional RNA Library Prep
795 Kit for Illumina® using the protocol for use with rRNA Depleted FFPE RNA. The data was quantified
796 using Salmon Version1.5.0 and tximport was used to obtain the transcript-level quantification. For
797 transcript classification, GENECODE annotation was performed.

798 **Fluorescence microscopy of fixed human or murine primary neutrophils**

799 500 µL of 1.6 x 10^6 cells/mL of human blood PMNs, and 2 x 10^6 cells/mL murine BM-PMNs were
800 seeded in a 24-well plate containing poly-L-lysine-coated glass coverslips (Electron Microscopy
801 Sciences, 72292-04) and rested for 30 min before stimulation at 37°C and 5% CO_2 with the according
802 stimuli (as described above) for 3 h (human) or 16 h (murine), respectively, as adapted from
803 Brinkmann *et al*., 2004 (*1*). After stimulation, the cells were carefully washed with PBS and fixed with
804 fixation buffer (Biolegend, 420801) for 10 min at RT in the dark. Afterwards, the cells were blocked
805 with PBS containing 0.1% heat-inactivated diethylpyrocarbonate (DEPC) (Roth, K028.2), 10% chicken
806 serum (Normal Chicken Serum Blocking Solution S-3000, Biozol/Vectorlabs, VEC-S-3000-20), 0.1%
807 saponin (Applichem, A4518.0100), as well as 10 U/µL RNase inhibitor for 2 h at RT. The primary
808 antibodies (rRNA Y10b, hLL37, see Supplementary Table S3) were diluted 1:50 in blocking buffer and
809 subsequently incubated for 2 h at RT. Afterwards, the cells were washed three times with PBS
810 containing 0.1% heat inactivated DEPC and incubated with the secondary antibodies (see
811 Supplementary Table S3) in a 1:500 dilution in blocking buffer for 1 h. After repeated washing, the
812 cells were incubated with Hoechst 33342 (Thermo Fisher; 1 µg/mL) for 5 min to stain nuclear DNA.
813 Secondary antibodies alone did not yield any significant staining under identical staining and
814 acquisition conditions. The coverslips were mounted (ProLong™ Diamond Antifade Mountant,
815 Thermo Fisher, P36961) on glass slides and left to dry overnight at RT in the dark. Subsequently, the
816 samples were stored at 4°C before microscopy using a Zeiss LSM800 Confocal microscope (40x or 63x
817 magnification with z-stack acquisition, AiryScan mode) and image analysis using ImageJ-Win64 and
818 Zen Blue3 software was performed. For IF of ultrathin sections, coverslips were coated with a carbon
819 layer, glow-discharged and UV-treated overnight before cells were seeded. After incubation, the cells
820 were fixed in 2.5% glutaraldehyde in PBS for 2 h at room temperature followed by incubation at 4°C.
821 Samples were prepared by the progressive lowering of temperature method (PLT). Therefore, the
822 fixed cells were incubated in ethanol for infiltration of Lowicryl HM20, followed by UV polymerization
823 and subsequent sectioning into 50-60 nm ultrathin slices. Immunolabeling was performed by
824 incubation with anti-rRNA Y10b and anti-LL37 primary antibodies for 1 h at RT. Afterwards, the cells
825 were incubated with goat anti-mouse Cy3 and goat anti-rabbit AF488 in blocking buffer for 1 h at RT.
826 Following immunolabeling, the samples were treated with 1% uranyl acetate for 5 min at RT before
827 analysis using a Zeiss Axioplan microscope (63x objective, Olympus SIS cell software) and image/line
828 plot analysis was performed using ImageJ-Win64.

829 **Quantification of NET formation**

830 To quantify the formation of NETs, microscopy images were obtained using a Zeiss LSM800 Confocal
831 microscope with a 40x objective and 3x3 tiles acquisition. Three images per sample of three
832 biological replicates were taken. To quantify NET formation by using NET-related signal dispersion of
833 rRNA and DNA signal, ImageJ-Win64 software was used, and a threshold (Triangle threshold) was
834 applied as originally described (*54*). Particles were analyzed with a ROI (region of interest) manager
835 (size (micron^2): 100-infinity (pixel units); circularity 0.00-1.00) and average size and number of
836 particles (ROIs) were assessed. In NETs, RNA and DNA signals showed up in a greater number and
837 smaller size, making the usage of the ratio suitable as a measurement of NET-related signal
838 dispersion. In the case of using the DNA signal only to assess NET formation, ImageJ-Win64 software
839 was used to create a PNG image and a grid with 8x8 tiles was manually applied to the images. Tiles
840 containing extracellular DNA structures were manually counted in a blinded manner as NET-positive
841 tiles.

842 **Live fluorescence microscopy of enzymatic digest of human NETs**

843 500 µL of 1.6 x 10^6 cells/mL of human blood PMNs were seeded in a 4-well glass bottom microscopy
844 cell culture dish (Greiner, 627871) and rested for 30 min before stimulation at 37°C and 5% CO_2 with
845 PMA (600 nM) for 3 h. After stimulation, the medium was carefully removed and the cells were
846 washed with PBS before adding fresh culture medium (RPMI culture medium without phenol red
847 (Sigma-Aldrich, R7509)+10% FBS (heat inactivated, sterile filtered, TH Geyer, 11682258)). Hoechst
848 33342 (Thermo Fisher, 1 µg/mL) to stain nuclear DNA and SYTO RNAselect Green fluorescent dye
849 (Thermo Fisher, 50 µM) to stain naRNA was added to the cells, as well as RNase A (Thermo Fisher,
850 EN0531; 100 µg/mL) was added between time point 0 and 5 min. Live cell imaging was performed
851 using a Zeiss LSM800 Confocal microscope with a 63x objective and z-stack acquisition, taking an
852 image every 5 min for 30-60 min respectively. Image analysis and video creation was performed
853 using ImageJ-Win64.

854 **Click chemistry of primary, stem cell-derived PMNs and fluorescence microscopy**

855 500 µL of 1.6 x 10^6 cells/mL of human stem cell-derived PMNs treated with 5-ethynyluridine or left
856 untreated were seeded in a 24-well plate containing poly-L-lysine-coated glass coverslips and rested
857 for 30 min before stimulation with PMA (600 nM) at 37°C and 5% CO_2 for 12 h. After stimulation, the
858 cells were washed and permeabilized with ice-cold acetone (Applichem, A1582.2500PE) 1:1
859 methanol (Honeywell, 32213-2.5L) for 5 min at RT. Subsequently, the click chemistry (reagents see
860 Supplementary Table S4) labeling of endogenous RNA was performed as described (*18*). Briefly, in a
861 total volume of 500 µL, 2 µL of AF546-Azide, a pre-mixture of 1 mM $CuSO_4$ and 1.25 mM THPTA, 5
862 mM aminoguanidine-hydrochloride and 5 mM Na-ascorbate in PBS were added to the cells in a 24-
863 well plate. The wells were sealed with plastic foil and incubated for 1 h at RT while shaking in the
864 dark. For negative controls, 5-ethynyluridine untreated cells incubated with complete click chemistry
865 reagents and 5-ethynyluridine treated cells incubated with PBS and AF546-Azide only were used. No
866 significant signals were observed. After the incubation, the cells were washed three times for 5 min
867 with PBS and counterstained with rRNA Y10b-AF647 (see Supplementary Table S3) at 1:50 in PBS for
868 2 h at RT in the dark. After repeated washing, the cells were incubated with Hoechst 33342 to stain
869 nuclear DNA and mounted as described above. Imaging and analysis were performed as previously
870 described.

871 **Electron microscopy**

872 For electron microscopy, 500 µL of 1.6 x 10^6 cells/mL of human blood-derived PMNs were seeded in a
873 24-well plate containing coverslips which were pre-coated with 0.01 % poly-L-lysine (Sigma, A-005-C)
874 for 15 min at 37°C for scanning electron microscopy (SEM). For transmission electron microscopy
875 (TEM), coverslips were coated with a carbon layer, glow-discharged and UV-treated overnight before
876 cells were seeded. Cells were rested for 30 min at 37°C and 5% CO_2 and subsequently stimulated with
877 1200 nM PMA or left untreated for 3 h. Afterwards, the cells were fixed in 2.5% glutaraldehyde in

878 PBS for 2 h at room temperature followed by incubation at 4°C. For SEM, samples were post-fixed
879 with 1% osmium tetroxide for 1 h on ice. Subsequently, samples were dehydrated in a graded
880 ethanol series followed by critical point drying (CPD300, Leica Microsystems) with CO_2. Finally, the
881 cells were sputter-coated with a 4 nm thick layer of platinum (CCU-010, Safematic) and examined
882 with a field emission scanning electron microscope (Regulus 8230, Hitachi High Technologies) at an
883 accelerating voltage of 3 kV. For antibody labeling, cells treated as described above were fixed in 4%
884 formaldehyde in PBS for 1-2 hours at room temperature and 4°C overnight. After washing and
885 blocking (0.2% gelatin in PBS) samples were incubated for 1 h at room temperature with rRNA Y10b
886 as the primary antibody in blocking buffer and for 1 h at RT with goat anti-mouse antibodies coupled
887 to 6 nm gold in blocking buffer (Jackson ImmunoResearch, code number 115-195-166). Samples
888 labeled with 6 nm gold were further silver enhanced. Following immunolabeling, the samples were
889 treated with 1% uranyl acetate for 5 min at RT, dehydrated and critical point dried as before.
890 Samples were sputter-coated with a 5 nm thick layer of carbon (CCU-010, Safematic) and analyzed in
891 the SEM with an accelerating voltage of 5 kV. For TEM, samples were prepared by the PLT method as
892 described above for IF of ultrathin sections. Samples were placed on grids (Cu, Ni) and subsequently
893 sectioned into 50-60 nm ultrathin slices. Immunolabeling was performed by incubation with anti-
894 rRNA Y10b as the first primary antibody in blocking buffer at 4°C overnight, followed by incubation
895 with anti-LL37 as the second primary antibody for 1 h at RT. Afterwards, the cells were incubated
896 with goat anti-mouse coupled to 6 nm gold and goat anti-rabbit 12 nm gold secondary antibodies in
897 blocking buffer for 1 h at RT. Following immunolabeling, the samples were treated with 1% uranyl
898 acetate for 5 min at RT before analysis in the TEM.

899

900 **Transient transfection of HEK293T cells**

901 HEK293T cells were transiently transfected with the respective TLR8, TLR7, TLR9 and NF-κB reporter
902 plasmids as described (*20*) (see Supplementary Table S5 for plasmids) using X-tremeGENE™ HP DNA
903 Transfection Reagent (Merck, 6366236001). A total amount of 5 x 10^4 cells/well were seeded in a 24-
904 well plate one day prior to transfection. For the transfection of one well, 100 ng of the according TLR
905 plasmid, 100 ng of the firefly luciferase NF-κB reporter and 10 ng *Renilla* luciferase control reporter
906 was mixed in Opti-MEM™ Reduced Serum Medium (Thermo Fisher, 31985062) in a total volume of
907 50 µL. After 15 min incubation at RT, the transfection mix was added to the cells and the cells were
908 incubated for 48 h. Prior to subsequent stimulation, the medium was changed to complete DMEM
909 medium (Sigma, D5796-24X500ML), and the cells were incubated with the respective NET content
910 stimuli and controls (R848 (2.5 µg/mL), TL8 (100 ng/mL), CpG (1.25 µM) + DOTAP (25 µg/mL), ssRNA
911 (0.6 µg/mL) + DOTAP (20 µg/mL), mock NETs + RNase inhibitor (1:50 dilution), PMA NETs (1:50
912 dilution), PMA NETs + RNase inhibitor (1:50)) for 18 h at 37°C and 5% CO_2. Supernatants were then
913 removed, and the cells frozen briefly at -80 °C. Subsequently they were used for dual luciferase assay.

914 **Dual luciferase reporter assay**

915 The dual luciferase reporter assay for detection NF-κB activation after TLR transfection and
916 subsequent stimulation was performed as described (*8*). In brief, supernatants were removed from
917 the cells after stimulation and 60 µL/well of 1x passive lysis buffer (E194A, Promega) was added. The
918 plate was then incubated for 15 min at RT on the plate shaker and subsequently stored at −80°C for
919 at least 15 min to facilitate complete cell lysis. After thawing, the cell solution (60 µL) was
920 transferred into a V-bottom 96-well plate and centrifuged for 10 min at 2500 rpm and 4°C to pellet
921 cell debris. Ten microliters of supernatant were then transferred into a white microplate and each
922 condition was measured in triplicates using the FLUOstar OPTIMA device (BMG Labtech). Firefly and
923 Renilla luciferase activity were determined using the Promega Dual luciferase kit. Both enzyme
924 activities were measured for 12.5 s with 24 intervals of 0.5 s, respectively. The data was analyzed by
925 calculating the ratio of the two measured signals, thereby normalizing each firefly luciferase signal to
926 its corresponding Renilla luciferase signal. The ratios were represented as the relative light units
927 (RLU) of NF-κB activation.

928 **Extracellular bacterial killing of *S. aureus***

929 The killing assay of *S. aureus* with human PMNs was performed according to Brinkmann *et al*., 2004
930 (*1*). In brief, PMNs were seeded at a density of 2 x 10^6 cells/mL and incubated with PMA (600 nM) for
931 2 h at 37°C. Afterwards, the medium was carefully replaced with serum-free culture medium,
932 containing 2% heat-inactivated pooled human serum with cytochalasin D (10 µg/mL) and incubated
933 further for 15 min before infection with bacteria. Cytochalasin D treatment did not affect NETs and
934 this concentration was effective in blocking bacterial phagocytosis. To investigate whether naRNA of
935 NETs was important in extracellular killing, samples were either treated with RNase A (Thermo
936 Fisher, EN0531; 100 µg/mL) or DNase I (Thermo Fisher, EN0521; 1 U/10 µL) for 2 h during NET
937 formation, or after NET formation during the 30 min bacterial killing process. Samples were
938 centrifuged at 700 x g for 10 min and incubated at 37°C and 5% CO_2 for 30 minutes. Bacterial killing
939 was measured as percentages of control values (bacteria incubated alone in media without
940 neutrophils).

941 **In vivo analysis of naRNA DAMP effects**

942 To investigate the effect of NETs with or without RNase inhibitors and the respective TLR signaling,
943 20 µL of NET content and the respective controls were injected into the ears of C57BL/6 and *Tlr13*$^{-/-}$
944 mice intradermally on day 0. Afterwards, as a measure of inflammation, the ear thickness was
945 assessed using a manual caliper (0.01–10 mm, Peacock, Tokyo, Japan) until day 4.

946 **Neutrophil infiltration *in vivo* fluorescence imaging**

947 The *in vivo* experiment for investigating neutrophil infiltration was performed as described (*8*).
948 Briefly, LysM$^{EGFP/+}$ mice were injected intradermally with 20 µL of PMA or mock NET content or
949 respective controls. LysM$^{EGFP/+}$ mice were then anesthetized with inhalation isoflurane and *in vivo*
950 fluorescence imaging was performed using the IVIS Lumina II imaging system (Caliper). EGFP
951 fluorescence was measured using excitation (465 nm), emission (515–575 nm), and exposure time
952 (0.5 s). Data are quantified as total radiant efficiency ([photons/s]/[µW/cm^2]) within a circular region
953 of interest using Living Image software (Caliper).

954 **Imiquimod model of psoriatic skin inflammation**

955 To analyze the effect of RNA signaling in an *in vivo* model for psoriasis, the well-established
956 imiquimod mouse model was used (*31*). C57BL/6 and *Tlr13*$^{-/-}$ mice were used and, briefly, 70 µL (62.5
957 mg) of imiquimod (5%, Taro Pharmaceuticals Industries, Hawthorne, NY) was applied daily to both
958 sides of a mouse ear for 5 consecutive days (day 0 to 4). Ear thickness was measured with a manual
959 caliper (0.01–10 mm, Peacock, Tokyo, Japan) before imiquimod application. A day after the last
960 application of imiquimod (day 5), full-thickness ear skin was excised with surgical scissors for
961 histologic analysis.

962 **Histologic analysis of mouse ear skin**

963 Ear skin specimens were collected by excising the entire ear with surgical scissors, fixed in formalin
964 (10%), and embedded in paraffin. 4 µm thickness sections were mounted onto glass slides and
965 stained with H&E by the Johns Hopkins Reference Histology Laboratory. To measure epidermal
966 thickness, 100 epidermal thickness measurements per mouse were averaged from images taken at
967 ×200 magnification (Hamamatsu Nanozoomer) using ImageJ software (NIH).

968 **ELISA**

969 To measure cytokine release of BlaER-1, THP-1, N/TERT-1, NHEK, NK-92 MI, PBMCs and 3D human
970 skin equivalent after stimulation with NET content and respective controls, ELISA Kits for hIL-8 (ELISA
971 MAX™ Deluxe Set Human IL-8, Biolegend, 431504), hIL-6 (ELISA MAX™ Deluxe Set Human IL-6,
972 Biolegend, 430504), IFN-γ (ELISA MAX™ Deluxe Set Human IFN-γ, Biolegend, 430104), and TNF (TNF
973 alpha Human Uncoated ELISA Kit, Invitrogen, 88-7346-88) were used according to the manufacturer's
974 instructions. Samples were assessed in triplicates.

975 **qPCR analysis of IL-8 expression of 3D human skin equivalent**

976 To investigate IL-8 expression of 3D human skin equivalent after stimulation with NET contents, qPCR
977 analysis was performed. First, total RNA was isolated using the RNeasy Mini Kit (Qiagen, 74106) for
978 animal tissues and cells. For cDNA preparation, the High-Capacity RNA-to-cDNA-Kit (Thermo Fisher,
979 4387406) was used according to the manufacturer's instructions. For the qPCR, the TaqMan™ system
980 was used. Briefly, a master mix of TaqMan™ Universal Mastermix II (Thermo Fisher, 4440040) and
981 TaqMan™ Gene Expression Assay (Thermo Fisher, 4448892) was prepared according to the
982 manufacturer's instructions. For one reaction, 5.5 µL master mix and 4.5 µL of the respective cDNA
983 (IL-8 and TBP) were mixed and the qPCR was run. Analysis in triplicates was performed using
984 QuantStudio Real-Time-PCR software version 1.3 (Thermo Fisher).

985 **Statistics**

986 Experimental data were analyzed using Excel 2019 (Microsoft) and/or GraphPad Prism 8, microscopy
987 data with ImageJ-Win64 or ZenBlue3 software, flow cytometry data with FlowJo V10. Normal
988 distribution in each group was always tested using the Shapiro–Wilk test first for the subsequent
989 choice of a parametric (ANOVA, Student's t-test for normally distributed data) or non-parametric
990 (Mann–Whitney U) test as indicated in figure legends. p-values ($\alpha = 0.05$) were then calculated, and
991 multiple testing was corrected for in Prism, as indicated in the figure legends. Values < 0.05 were
992 generally considered statistically as significant and denoted by * throughout even if considerably
993 lower. Comparisons made to unstimulated control, unless indicated otherwise, were denoted by
994 brackets.

995 **Supplementary figures**

996 **Fig. S1: Controls of IF microscopy, stem cell-derived PMNs, and electron microscopy**

997 **(A)** Confocal microscopy of unstimulated primary human PMNs (control to Fig. 1A) after 3 h and
998 stained for naRNA (anti-rRNA Y10b, magenta) and DNA (Hoechst 33342, white, n = 3, representative
999 images, scale bar: 10 µm). **(B)** Confocal microscopy of unstimulated primary murine BM-PMNs
1000 (control to Fig. 1C) after 16 h and stained as in **A** (n = 3, representative images, scale bar: 10 µm). **(C)**
1001 Brightfield microscopy analysis of cytospun control primary human stem cell-derived PMNs (control
1002 to Fig. 1D) differentiated *in vitro* with/without 100 µM 5-Ethynyluridine (5-EU, n = 3, representative
1003 images, scale bar: 20 µm). **(D)** FACS analysis for cells shown in **C** and Fig. 1D (n=3, representative
1004 data). **(E)** Scanning electron microscopy of PMA-treated human primary PMNs showing only
1005 secondary antibody staining (no primary antibody) control of Fig. 1F (n = 1, representative data; the
1006 image on the right is a composite image with signals from secondary electron and backscattered
1007 electron detectors for topography and additional material information, respectively).

1008 **Fig. S2: Antibacterial effect of NETs on live *S. aureus*, controls of IF microscopy and line plot**
1009 **analysis of naRNA and LL37**

1010 **(A)** Extracellular bactericidal activity of human PMNs/NETs after infection with *S. aureus* and
1011 treatment with RNase A and DNase I during or after formation of PMA-induced NETs (n = 8,
1012 combined data, mean+SD, *p<0.05 according to one-way ANOVA). **(B)** Confocal microscopy of
1013 unstimulated or PMA-stimulated primary human PMNs (control to Fig. 2B) after 3 h, stained DNA
1014 (Hoechst 33342, white, n = 9, representative images, scale bar: 10 µm). **(C)** as in **B** but controls of Fig.
1015 2D (n = 3). **(D)** As in **B** but controls of Fig. 2F (n = 3).

1016 **Fig. S3: Inhibition of PAD4 in human PMNs during NET formation assay and *Unc93b1*$^{-/-}$ and *Tlr9*$^{-/-}$**
1017 **BM-PMN stimulation with human NETs**

1018 **(A)** Confocal microscopy of stimulated primary human PMNs after 3 h and stained for DNA (Hoechst
1019 33342, white) in the presence or absence of the PAD4-inhibitor Cl-amidine (200 µM, n = 3,
1020 representative images; scale bar 10 µm). **(B)** Confocal microscopy of primary C57BL/6 WT or
1021 *Unc93b1*$^{-/-}$ murine BM-PMNs stimulated as indicated for 16 h as in **A** (n = 3 WT, n = 1 *Unc93b1*$^{-/-}$,
1022 representative images, scale bar: 10 µm). **(C)** Confocal microscopy of primary C57BL/6 WT or *Tlr9*$^{-/-}$
1023 murine BM-PMNs stimulated as indicated for 16 h as in **A** (n = 3, representative images, scale bar: 10
1024 µm).

1025 **Fig. S4: Immune responses of PBMCs, macrophages, and NK-cells to NETs and in vivo fluorescence**
1026 **imaging**

1027 **(A)** Triplicate IL-8 ELISA from WT, *TLR8*$^{-/-}$ and *TLR7*$^{-/-}$ THP-1 cells stimulated as indicated for 18 h,
1028 normalized to PMA+ionomycin control (n = 4, combined data, mean+SD, each dot represents one

1029 biological replicate, *p<0.05 according to one-way ANOVA). **(B-D)** Triplicate ELISA for TNF (**A**, n = 4),
1030 IL-6 (**B**, n = 3), and IL-8 (**C**, n = 3) from primary human PBMCs stimulated as indicated with/without
1031 CU-CPT9a for 24 h (combined data, mean+SD, each dot represents one biological replicate, *p<0.05
1032 according to one-way ANOVA). **(E)** Triplicate IFN-γ ELISA from NK-92 MI cells stimulated as indicated
1033 for 24 h (n = 3, combined data, mean+SD, each dot represents one biological replicate, *p<0.05
1034 according to one-way ANOVA).

1035 **Fig. S5: Pre-association of naRNA and LL37 in resting healthy donor neutrophils**

1036 **(A)** Confocal microscopy of primary human PMNs stimulated as indicated for 3 h and stained for
1037 naRNA (anti-rRNA Y10b, magenta), LL37 (anti-hLL37-DyLight550, yellow) and DNA (Hoechst 33342,
1038 white, n = 3, representative images). The line plot analysis of LL37, RNA and DNA staining was
1039 performed using ZenBlue3 software. Two to three different line plots from the same representative
1040 image are shown. **(B)** Transmission electron microscopy of unstimulated human primary PMNs using
1041 anti-rRNA and anti-hLL-37 primary and immunogold (6 nm (black arrow) and 12 nm (white arrow)
1042 respectively)-labeled secondary antibodies (n = 3, representative images, scale bars as indicated).

1043 **Fig. S6. Graphical abstract**

1044 **Supplemental movies**

1045 **Supplemental movie S1: 3D reconstruction of NET DNA network decorated with naRNA**

1046 Confocal microscopy of primary human PMNs stimulated with PMA for 3 h, stained for naRNA (anti-
1047 rRNA Y10b, magenta) and DNA (Hoechst 33342, white, n = 3) and 3D analysis and animation were
1048 performed using ZenBlue3 software.

1049 **Supplemental movie S2: Digest of naRNA in PMA-induced NETs**

1050 Confocal live microscopy of RNase digestion of NETs obtained from primary human PMNs stimulated
1051 with PMA for 3 h, stained for naRNA (SYTO RNAselect, magenta) and DNA (Hoechst 33342, white, n =
1052 3). RNase A was added between time point 0 and 5 min (n = 3, scale bar 20 µm). Video analysis and
1053 animation were performed using ImageJ-Win64 software.

1054 **Supplementary Tables**

1055 **Supplementary Table 1: commercial TLR ligands and inhibitors; enzymes**

Component	Company	Product no.
Cl-amidine	Merck	506282
CpG PTO 2006	TIB Molbiol	n/a, see Table S2
CU-CPT9a	Invivogen	inh-cc9a
DNase I	Thermo Fisher	EN0521
DNase inhibitor 50 mM EDTA	Thermo Fisher	EN0521
DOTAP	Roth	L787.2
Ionomycin	Sigma	I0634-1MG
LL37	Invivogen	tlrl-ll37
LPS-EK (ultrapure)	Invivogen	tlrl-peklps
Nigericin	Invivogen	tlrl-nig
PMA	Invivogen	tlrl-pma
R848 (Resiquimod)	Invivogen	tlrl-r848
RNase A	Thermo Fisher	EN0531
RNase inhibitor	Promega	N2615
TL8-506	Invivogen	tlrl-tl8506

1056

1057 **Supplementary Table 2: Nucleic acid TLR agonists**

Component	Sequence	Backbone	Company
RNA40	5'GsCsCsCsGsUsCsUsGsUsUsGsUsGsUsGsAsCsUsC3'	Phosphorothioate	Eurogentec
CpG PTO 2006	5'TsCsGsTsCsGsTsTsTsTsGsTsCsGsTsTsTsTsGsTsCsGsTsT3'	Phosphorothioate	TIB

1058

1059 **Supplementary Table 3: Antibodies and conjugation kit**

Item	Fluorophore	Species	Isotype	Company	Product no.
Anti-hLL37	DyLight 550	rabbit	IgG	LSBio	LS-B6696-500
DyLight 550 Conjugation Kit (Fast)	DyLight 550	-	-	Abcam	ab201800

Anti-rRNA (Y10b)	unconjugated	mouse	IgG_{2a} κ	Santa Cruz Biotechnology	sc-33678
Anti-rRNA (Y10b) Alexa Fluor® 647	AF647	mouse	IgG_{2a} κ	Santa Cruz Biotechnology	sc-33678 AF647
Anti-mouse IgG	AF647	chicken	IgY	Thermo Fisher	A-21463
Hoechst 33342	-	-	-	Thermo Fisher	H21492
SYTO RNAselect Green fluorescent dye	-	-	-	Thermo Fisher	S32703
Anti-mouse Cy3	Cy3	goat	IgG	Jackson ImmunoResearch	115-165-146
Anti-rabbit AF488	AF488	goat	IgG	Molecular Probes	A-11008
Anti-mouse 6 nm gold	-	goat	IgG	Jackson ImmunoResearch	115-195-166
Anti-rabbit 12 nm gold	-	goat	IgG	Jackson ImmunoResearch	111-205-144

1060

1061 **Supplementary Table 4: Click chemistry reagents**

Reagent	Company	Product no.
AF546-Azide	Jena Bioscience	CLK-1283-1
Aminoguanidine-Hydrochloride	Merck	396494-25G
$CuSO_4$-click chemistry grade	Jena Bioscience	CLK-MI004-50.1
5-Ethynyluridine	Jena Bioscience	CLK-N002-10
Na-Ascorbate-click chemistry grade	Jena Bioscience	CLK-MI005-1G
THPTA (Tris((1-hydroxy-propyl-1H-1,2,3-triazol-4-yl)methyl)amine)	Jena Bioscience	CLK-1010-25

1062

1063 **Supplementary Table 5: Plasmids used for HEK293T transfection**

Plasmid name insert	Vector backbone	Insert
NF-κB reporter	pGL3	6x NF-κB response element
Renilla	pRL-TK	*Renilla*
hTLR7	pcDNA3.1 (+)	hTLR7
hTLR8	pcDNA3.1 (+)	hTLR8
hTLR9	pSEM-hTLR9	hTLR9

1064

1065 **Supplementary Table 6: primers used for qPCR**

Gene	Assay number
IL-8	Hs00174103_m1
TBP (housekeeper)	HS00427620_m1

1066

1067 **Supplementary Table 7: 10x Ammonium chloride erythrocyte lysis buffer**

Compound	Company	Product no.
1.54 M NH_4Cl	Roth	5470.1
100 mM $KHCO_3$	Fluka	60220
1 mM EDTA; pH 8 dissolved in Ampuwa water	Thermo Fisher Fresenius Kabi	15575020 1833
pH adjusted to 7.3, sterile filtered (0.22 µm)		

1068

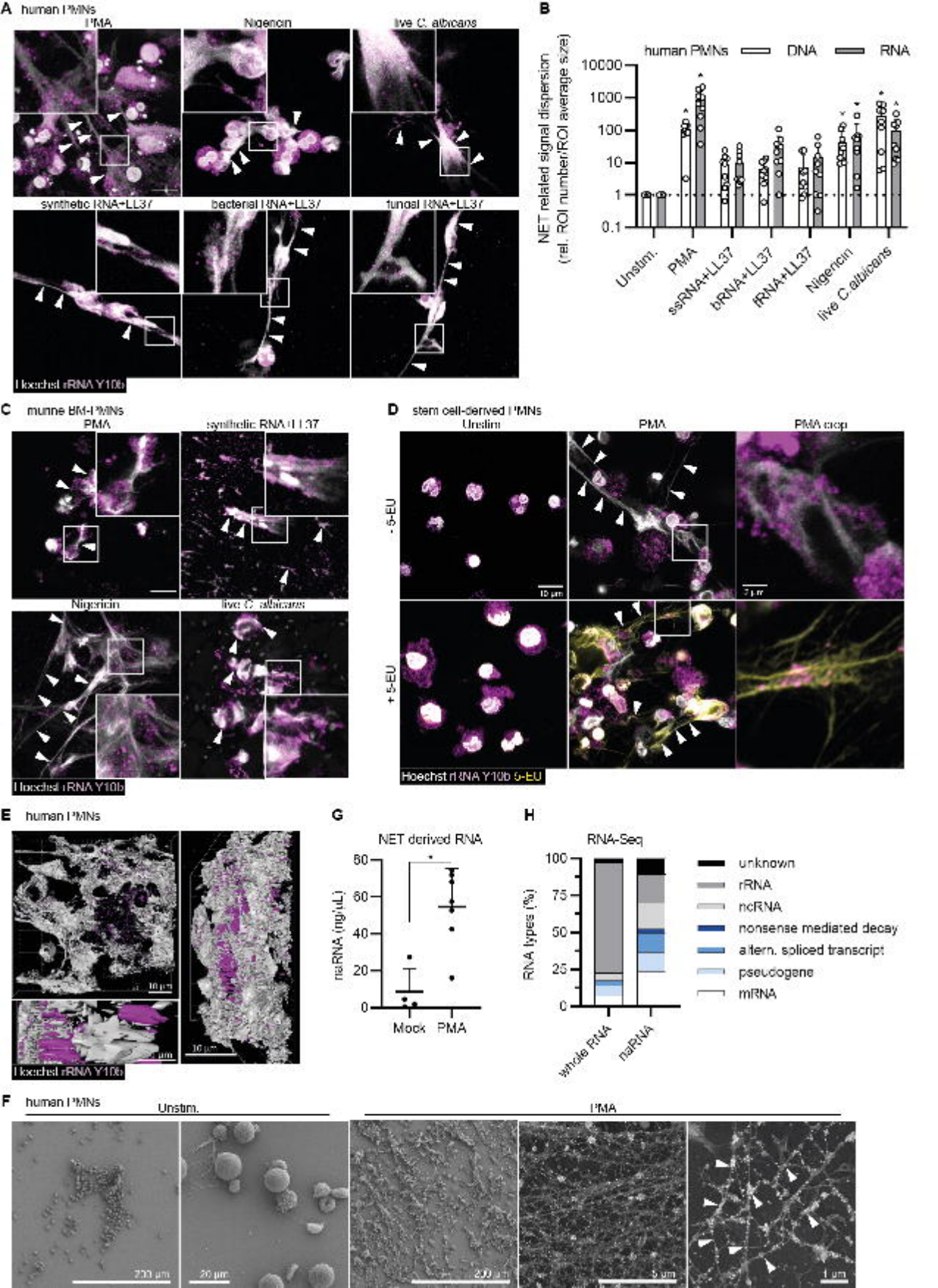
A
human PMNs
PMA
Nigericin
live C. albicans
synthetic RNA+LL37
bacterial RNA+LL37
fungal RNA+LL37
Hoechst rRNA Y10b
B
human PMNs
DNA
RNA
NET related signal dispersion (rel. ROI number/ROI average size)
10000
1000
100
10
1
0.1
Unstim.
PMA
ssRNA+LL37
bRNA+LL37
fRNA+LL37
Nigericin
live C. albicans
C
murine BM-PMNs
PMA
synthetic RNA+LL37
Nigericin
live C. albicans
Hoechst rRNA Y10b
D
stem cell-derived PMNs
Unstim.
PMA
PMA zoom
- 5-EU
+ 5-EU
10 µm
Hoechst rRNA Y10b 5-EU
E
human PMNs
10 µm
Hoechst rRNA Y10b
G
NET derived RNA
naRNA (ng/µL)
80
60
40
20
0
Mock
PMA
H
RNA-Seq
RNA types (%)
100
75
50
25
0
whole RNA
naRNA
unknown
rRNA
ncRNA
nonsense mediated decay
altern. spliced transcript
pseudogene
mRNA
F
human PMNs
Unstim.
PMA
200 µm
20 µm
200 µm
5 µm
1 µm

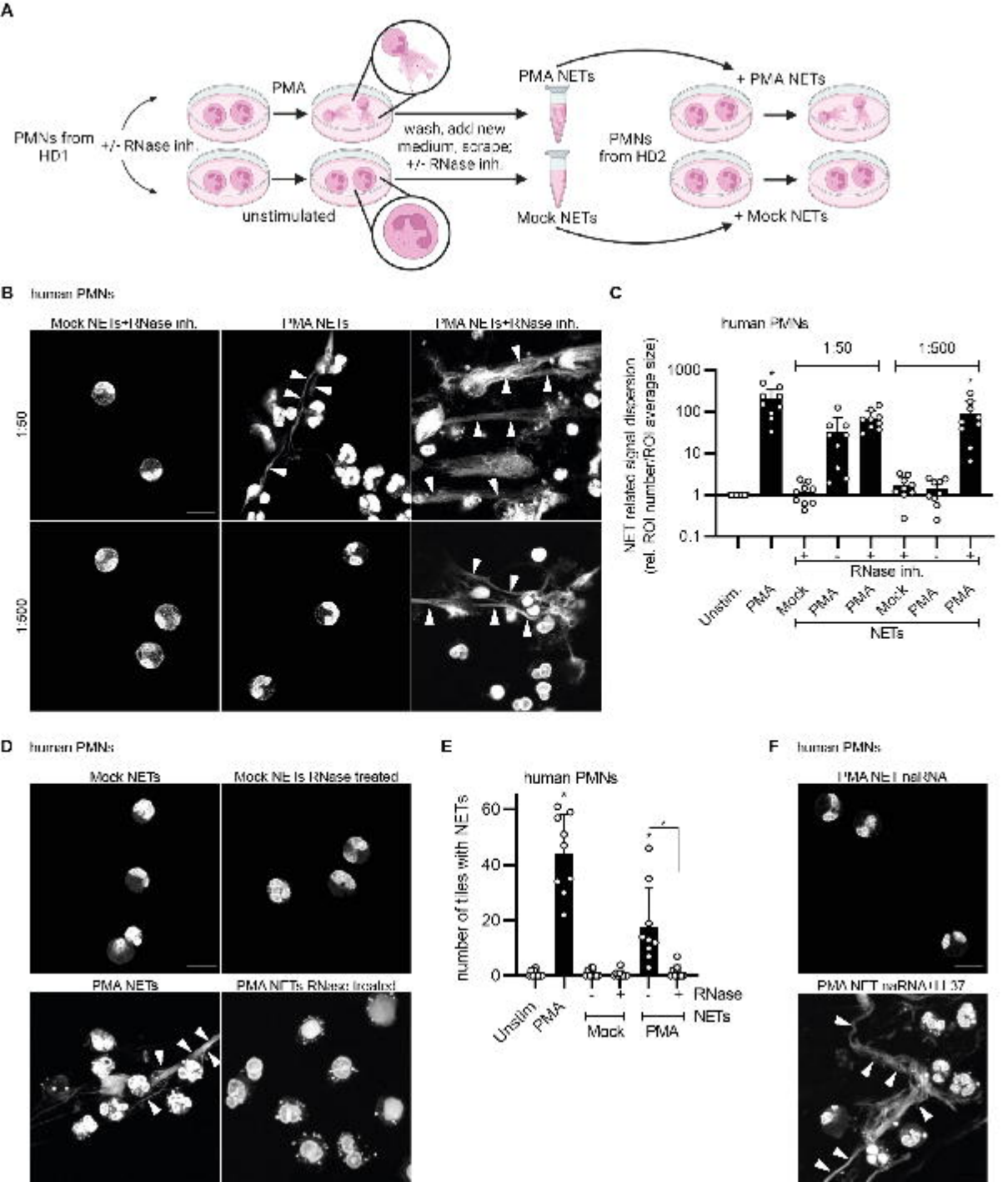
A
PMNs from HD1
+/- RNase inh.
PMA
unstimulated
wash, add new medium, scrape; +/- RNase inh.
PMA NETs
Mock NETs
PMNs from HD2
+ PMA NETs
+ Mock NETs
B
human PMNs
Mock NETs+RNase inh.
PMA NETs
PMA NETs+RNase inh.
1:50
1:500
C
human PMNs
NET related signal dispersion (rel. ROI number/ROI average size)
1:50
1:500
RNase inh.
Unstim.
PMA
Mock
NETs
D
human PMNs
Mock NETs
Mock NETs RNase treated
PMA NETs
PMA NETs RNase treated
E
human PMNs
number of tiles with NETs
RNase
NETs
Unstim
PMA
Mock
PMA
F
human PMNs
PMA NET nsRNA
PMA NET miRNA LL37

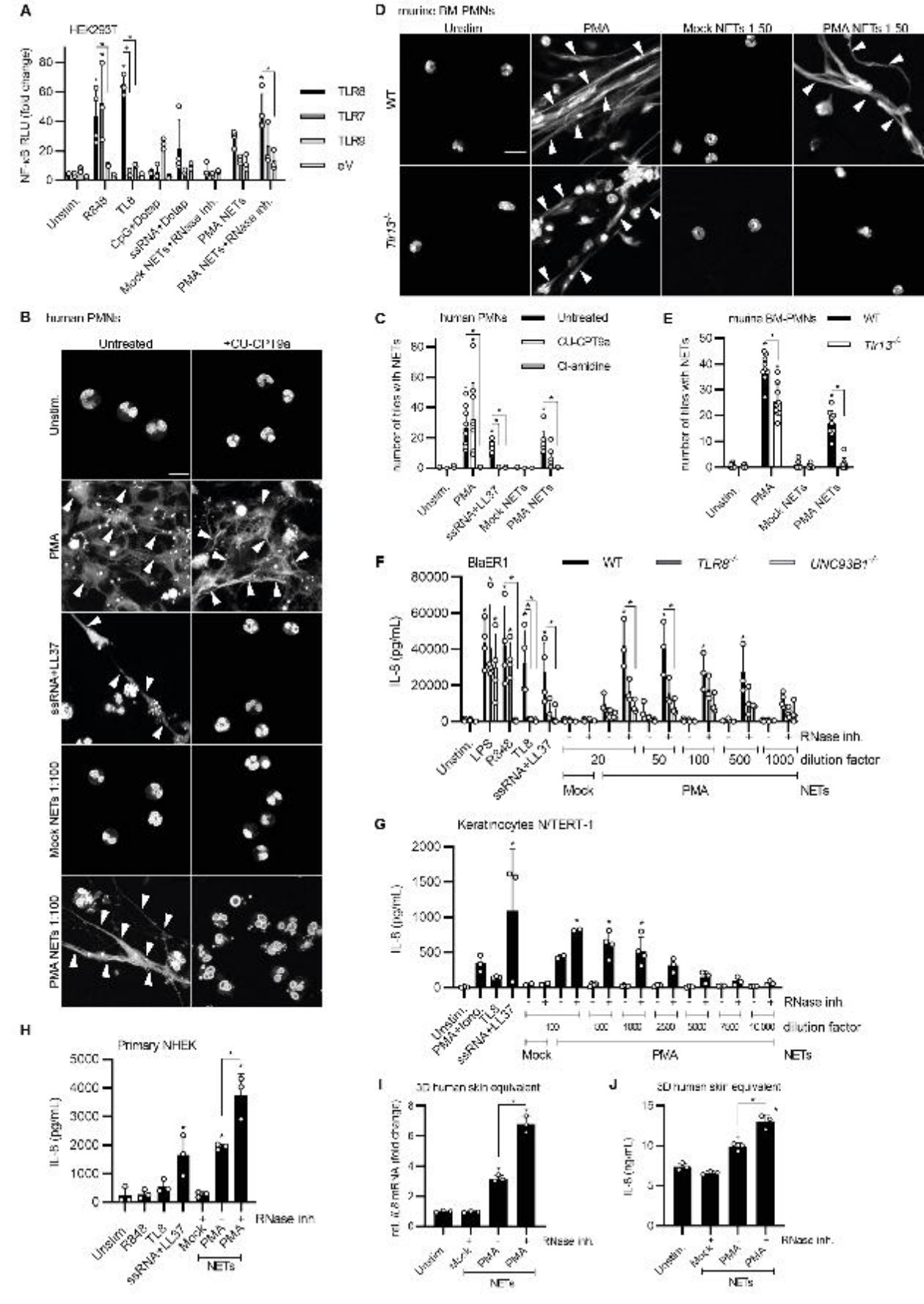
A
HEK293T
NF-κB RLU (fold change)
TLR8
TLR7
TLR9
eV
Unstim.
R848
TL8
CpG+Dotap
ssRNA+Dotap
Mock NETs+RNase inh.
PMA NETs
PMA NETs+RNase inh.
B
human PMNs
Untreated
+CU-CPT9a
Unstim.
PMA
ssRNA+LL37
Mock NETs 1:100
PMA NETs 1:100
C
human PMNs
Untreated
CU-CPT9a
Cl-amidine
number of lies with NETs
Unstim.
PMA
ssRNA+LL37
Mock NETs
PMA NETs
D
murine BM PMNs
Unstim
PMA
Mock NETs 1:50
PMA NETs 1:50
WT
Tlr13-/-
E
murine BM-PMNs
WT
Tlr13-/-
number of lies with NETs
Unstim.
PMA
Mock NETs
PMA NETs
F
BlaER1
WT
TLR8-/-
UNC93B1-/-
IL-8 (pg/mL)
Unstim.
LPS
R848
TL8
ssRNA+LL37
RNase inh.
20
50
100
500
1000
dilution factor
Mock
PMA
NETs
G
Keratinocytes N/TERT-1
IL-8 (pg/mL)
Unstim.
PMA+topo.
TL8
ssRNA+LL37
RNase inh.
100
500
1000
2500
5000
7500
10 000
dilution factor
Mock
PMA
NETs
H
Primary NHEK
IL-8 (pg/mL)
Unstim.
R848
TL8
ssRNA+LL37
Mock
PMA
PMA
RNase inh.
NETs
I
3D human skin equivalent
rel. il8 mRNA (fold change)
Unstim.
Mock
PMA
PMA
RNase inh.
NETs
J
3D human skin equivalent
IL-8 (pg/mL)
Unstim.
Mock
PMA
PMA
RNase inh.
NETs

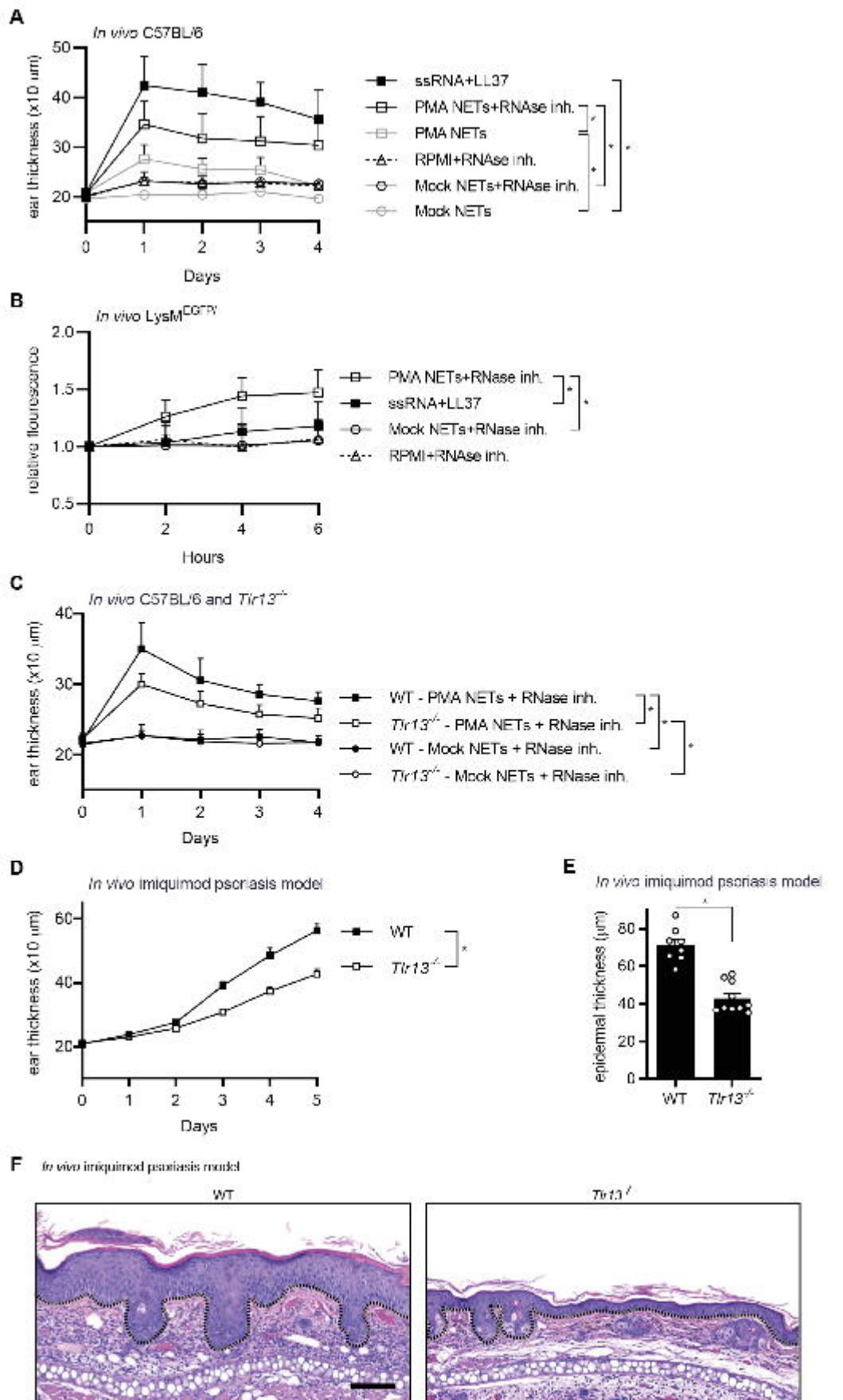
A
In vivo C57BL/6
ear thickness (x10 um)
Days
ssRNA+LL37
PMA NETs+RNAse inh.
PMA NETs
RPMI+RNAse inh.
Mock NETs+RNAse inh.
Mock NETs
B
In vivo LysM^EGFP
relative flourescence
Hours
PMA NETs+RNase inh.
ssRNA+LL37
Mock NETs+RNase inh.
RPMI+RNAse inh.
C
In vivo C57BL/6 and Tlr13^-/-
ear thickness (x10 um)
Days
WT - PMA NETs + RNase inh.
Tlr13^-/- - PMA NETs + RNase inh.
WT - Mock NETs + RNase inh.
Tlr13^-/- - Mock NETs + RNase inh.
D
In vivo imiquimod psoriasis model
ear thickness (x10 um)
Days
WT
Tlr13^-/-
E
In vivo imiquimod psoriasis model
epidermal thickness (µm)
WT
Tlr13^-/-
F
In vivo imiquimod psoriasis model
WT
Tlr13^-/-

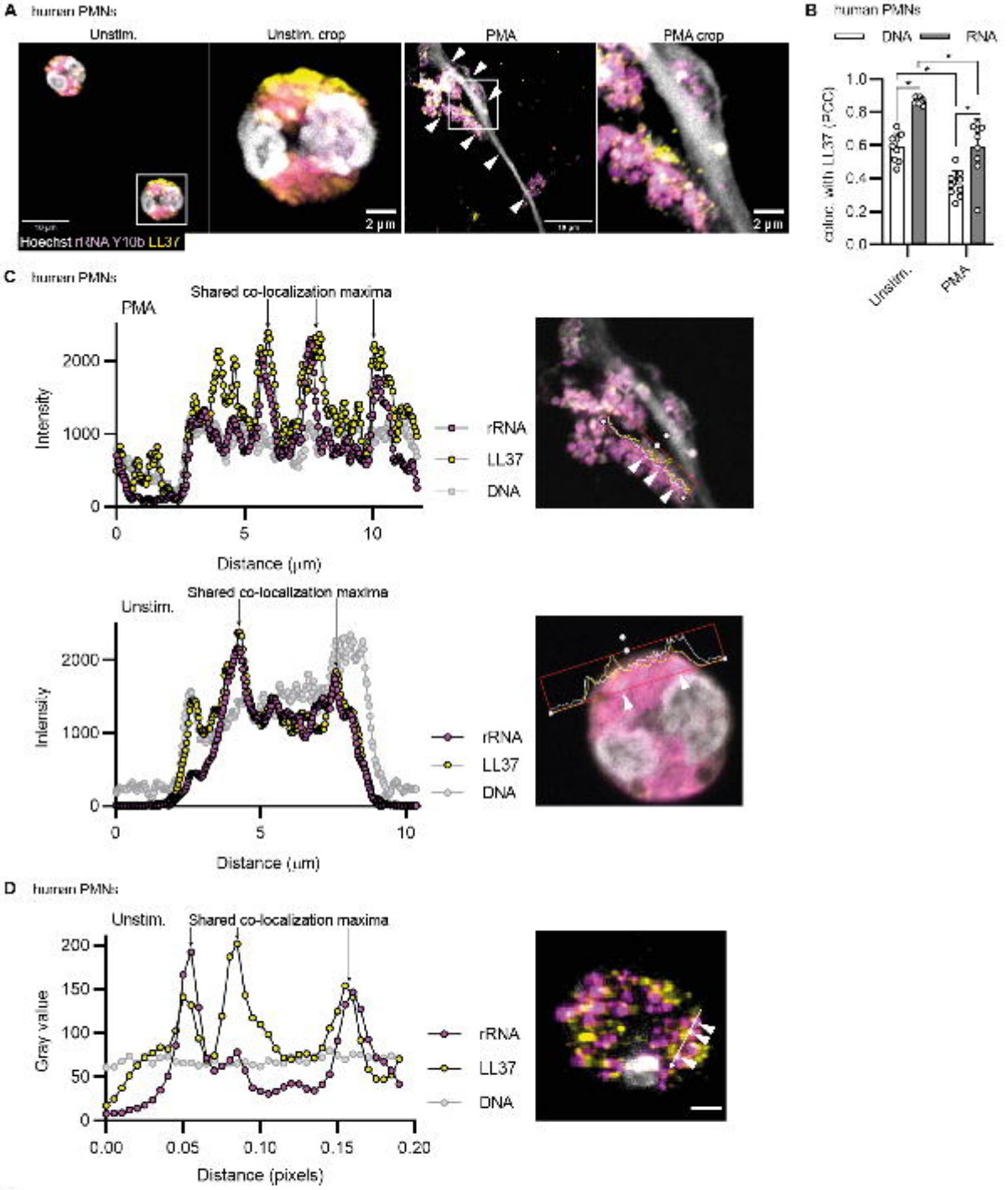
A human PMNs
Unstim.
Unstim. crop
PMA
PMA crop
2 µm
2 µm
Hoechst rRNA Y10b LL37
B human PMNs
DNA
RNA
coloc. with LL37 (PCC)
1.0
0.8
0.6
0.4
0.2
0.0
Unstim.
PMA
C human PMNs
PMA
Shared co-localization maxima
Intensity
2000
1000
0
0
5
10
Distance (µm)
rRNA
LL37
DNA
Unstim.
Shared co-localization maxima
Intensity
2000
1000
0
0
5
10
Distance (µm)
rRNA
LL37
DNA
D human PMNs
Unstim.
Shared co-localization maxima
Gray value
200
150
100
50
0
0.00
0.05
0.10
0.15
0.20
Distance (pixels)
rRNA
LL37
DNA
E human PMNs
5 µm
200 nm
5 µm
200 nm